Physics – Uspekhi **65** (6) 597 – 616 (2022)

REVIEWS OF TOPICAL PROBLEMS PACS numbers: 64.70.D –, **65.40. – b,** 81.05.Je

Physical properties of refractory carbides of metals of groups IV and V of the Mendeleev periodic table during rapid heating by an electric current pulse

A I Savvatimskiy, S V Onufriev, N M Aristova

DOI: https://doi.org/10.3367/UFNe.2021.06.038990

Contents

Abstract. A method for studying the thermophysical properties of refractory carbides under pulsed electric heating for 5–10 microseconds is considered. Results are presented for (ZrC; Zr + C; TaC + HfC; HfC) as a function of the temperature measured from ~ 2000 K to 5000 K. Data on enthalpy, specific heat C_p, heat of melting, and electrical resistance are given. For all the studied carbides, a sharp increase in the specific heat of the solid phase is observed at ≈ 300 K before melting. This may be due to the formation of paired Frenkel defects under conditions of a short heating time. Comparative data on the results obtained for all carbides are presented, and the choice of carbides for creating thermal protection is discussed.

Keywords: pulse heating, refractory carbides, melting temperature, liquid state, thermophysical properties, electrical resistance

1. Introduction

Carbides of metals of groups IV and V of the periodic system of elements — Zr, Hf, Ta — have a unique set of properties: very high melting points (above 3400 K), metallic conductivity, high thermal conductivity, high hardness, high elastic and shear moduli, and chemical inertia. These carbides belong to the group of super-fusible substances, which is commonly referred to in the literature as Ultra-High-Temperature Ceramics (UHTCs) [1]. UHTCs also include borides, nitrides, and oxides of substances with high melting points. It is noted in [1] that the combination of the properties of these carbides makes them promising materials for the development of high-temperature devices, including rocket engines, hypersonic aircraft, thermal protection elements, and high-temperature nuclear reactors. Carbides are considered to be the most refractory compounds. Recently, new composite materials (based on UHTCs) have been developed that have a higher resistance in the oxidizing air environment or in the environment of combustion products than UHTCs [2]. For the same purpose, various multicomponent ceramics are being developed. For example, in [3], a composition of a mixed carbide based on ZrC is proposed that is resistant to ablation at temperatures up to 3300 K.

New approaches to the development of refractory compounds, including nanostructured ones, are presented in [4, 5]. To evaluate the behavior of these materials at high temperatures, it is necessary to know the properties of the initial two-component solutions (carbides, nitrides, borides), both in the solid and in the liquid states.

Zirconium and hafnium, interacting with carbon, form only ZrC and HfC monocarbides. Tantalum forms carbides Ta_2C and TaC, of which TaC monocarbide is more stable and has a higher melting point (4223 K, [4]). These monocarbides have wide regions of homogeneity, i.e., they are compounds of variable composition, which are described by the formula MC_x, where M is a metal, C is carbon, and x varies widely, for example, $0.55 \leqslant x < 1$ for ZrC_x. The compounds have a face-centered cubic lattice. Carbon atoms are located in octahedral internodes, some of which remain unoccupied at $x < 1$.

There is an extensive literature, including references, devoted to the study of the properties of carbides. However, it should be noted that studies of properties at high

A I Savvatimskiy *, S V Onufriev, N M Aristova
Joint Institute for High Temperatures Russian Academy of Sciences, ul. Izhorskaya 13, str. 2, 125412 Moscow, Russian Federation
E-mail: * savvatimskiy.alexander@gmail.com

Received 22 March 2021, revised 1 June 2021
Uspekhi Fizicheskikh Nauk **192** (1) 642 – 662 (2022)
Translated by A I Savvatimskiy

temperatures, especially near melting, are few and often contradictory. The properties of the liquid phase of refractory carbides have remained unexplored until recently. Only estimates of the enthalpy and specific heat, as well as the heat of melting, have been calculated. The main properties of carbides at different temperatures are given in [6–11].

Information on the temperature dependences of properties obtained both experimentally and by calculation is collected in [12]. Modern experimental data on the thermophysical properties and radiative characteristics of carbides are presented in [13], and recommended temperature dependences of these properties are given. The results of classical measurements are also presented in [14].

Studies of the enthalpy, specific heat, electrical resistance of the solid and liquid phases of carbides in the temperature range from 2000 to 5000 K and measurements of the temperature and heat of melting were performed by heating an electric current pulse with a duration of 5–10 μs, which corresponds to a heating rate of $\sim 10^8 - 10^9$ K s^{-1} or ($10^2 - 10^3$ K μs^{-1}). Note that these heating rates look unusually large, but it is known that the time of electron-ion relaxation in a solid is several picoseconds (10–12 s). This is not only an estimate, for example [15], but also an experimental fact [16]. Thus, during microsecond heating, the electron and ion subsystems are in equilibrium with each other, giving grounds for applying the concept of local thermodynamic equilibrium to the description of the specimen state.

The question of the possible 'overheating' of a solid body above the melting point at a high heating rate is closely related to this problem. A possible increase in the melting temperature of pure metal was not confirmed in our direct measurement of the melting temperature of pure Ta [17], heated at a rate of 10^8 K s^{-1}. A successful experiment was performed in [18], where a diamond plate (500 μm thick) was melted when it was heated by a laser pulse with a duration of 1 ns, under conditions of megabar pressures. The melting point of the diamond (9000 K) corresponded to the measured pressure. The heating rate was $\sim 10^{11}$ K s^{-1}. An analysis of literary publications of recent years has shown that the alleged overheating of pure substances with rapid heating is unlikely.

At the same time, rapid current heating has a number of features — a sharp increase in the specific heat capacity of the solid phase is observed at ≈ 300 K before melting, which is common to all the studied carbides. The same effect was observed earlier when studying the properties of metals [19] and graphite [20] under rapid heating by current, i.e., perhaps this effect has a general nature with rapid heating of substances. The authors of these studies suggest that this effect may be associated with the formation of paired Frenkel defects under conditions of a short heating time.

Recent theoretical estimates by the molecular dynamics method at $T = 3200$ K for zirconium carbide [21] show the possibility of an increase in the specific heat due to the formation of Frenkel pairs even before the melting of the solid. In the same study, the contribution of Frenkel defects to the measured physical properties of ZrC is estimated.

It should be noted that, due to very high melting temperatures, it is almost impossible to perform such studies using traditional stationary methods. It is necessary to use rapid current heating, which has a number of advantages [22, 23] over standard stationary methods:

— the highest temperatures (above the boiling point of the material) are easily reached;

— the short duration of the heating process leads to small thermal losses of all types, amounting to a fraction of one percent of the Joule heating energy scattered in the sample, which makes it possible to measure thermal properties with acceptable accuracy;

— volumetric heating of the sample takes place under current action, and this allows its volumetric properties (such as enthalpy, specific heat, and resistivity) to be measured, which is impossible with laser heating;

— digital oscillography allows measuring several thermophysical properties simultaneously for the solid and liquid states of a substance in each individual experiment;

— the short duration of the heating process allows the stoichiometry of the sample composition to be preserved during heating and to be ignored the interaction of the sample with the environment.

The main results of studying the physical properties of refractory carbides in solid and liquid states when heated by a current pulse for 5–10 μs ($dT/dt \sim 5 \times 10^8$ K s^{-1}) are given in [24–31]. As noted in these publications, the method allows us to study the temperature dependences of the enthalpy, specific heat, and electrical resistance of a conducting substance in the solid phase during melting and in a wide range of the liquid state, as well as the temperature and enthalpy of phase transitions. The methods of powder metallurgy and coating methods were used for the production of specimens. Pulsed methods of current heating allowed us to reach a new level of temperature research of the properties of substances (up to 5000–8000 K). This is significantly higher than the capabilities of stationary studies. Apparently, the temperature of 3800 K can be considered the limit of the capacity of stationary studies [32].

2. Features of the study of the properties of carbides by the method of heating by a current pulse

The studies were performed with specimens in the form of thin plates (more massive samples) and of thin layers deposited on a dielectric substrate (optical glass K8 or silica glass). In the first case, the initial blanks were obtained by Spark Plasma Sintering (SPS method) of carbide powder. These blanks were cut by a diamond disk into plates with a thickness of 100–150 μm. In the second case, specimens in the form of a coating with a thickness of 1–10 μm were obtained by magnetron sputtering of a target also manufactured by the SPS method. The final specimens (plates and coatings) had different structures, porosities, and grain sizes. The plates had a grain size of about 10–15 μm, and the coatings had a grain size of about 1 μm or less.

The test specimen was placed in a cell between two glass plates (without the use of side glued glasses!) to prevent the occurrence of a surface discharge at high voltage along the specimen. During pulsed heating, a small pulsed pressure (about 5–10 MPa) appeared in the specimens, the influence of which can be ignored, and the Joule heat scattered in the sample can be considered equal to the enthalpy, while the measured specific heat is that at constant pressure. It should be noted here that the gluing of additional glasses along both sides of the cell leads to a significant increase in the pulse pressure, on the order of tens of kbar at short heating times (~ 1 μs; $dT/dt \sim 5 \times 10^9$ K s^{-1}); the issue is considered in [20].

In our case of coating, two cell variants were used: the first cell consisted only of a substrate on which the coating was

applied (experiments were carried out in water); in the second case, the coated substrate was covered from above with a glass plate (experiments were carried out in the air). The temperature was measured by the optical method using a high-speed pyrometer based on fast PDA-10A photodetectors (Thorlabs). In this case, we used the literature data on the emissivity of the studied substances. In their absence, a wedge-shaped model of a blackbody consisting of two glass plates covered with a thin layers of the studied carbide were used [24].

It should be noted that, with the exception of publications [24–31], there are no experimental data in the literature on the specific properties (for example, the specific heat) of refractory carbides in the liquid phase, which is associated with the very high melting temperatures of these substances. The behavior of the specific heat of all the carbides considered below has features previously discovered for metals [22, 23]. With rapid heating, 200–300 K before melting, the specific heat of these carbides increases abnormally. After melting, approximately in the same temperature range, it quickly falls, approaching the estimates obtained for equilibrium conditions.

It can be assumed that the anomalous increase in the specific heat of the solid phase of carbides (as well as of metals) in the melting region is associated with the rapid formation of nonequilibrium Frenkel defects and with an increase in the energy of the crystal lattice before melting. Immediately after the melting is completed, a sharp drop in the specific heat is observed, presumably due to the annihilation of excess defects. This leads to a drop in the specific heat to values close to equilibrium.

The development of the method of rapid pulsed heating by a current pulse has led to a wide application of the method for obtaining data on the physical properties of substances (metals, alloys, carbides, nitrides, and carbon) at high temperatures. The study temperatures reached 5000 K and higher (for example, up to 8000–12,000 K for liquid carbon). Indeed, such studies in stationary conditions are impossible. The method of fast heating, including temperature measurement using a high-speed pyrometer, is described in [33]. Temperature measurements were carried out at a wavelength of 856 nm. Errors in measuring the properties of the specimens were as follows: Joule heating energy (enthalpy) — 5–6%; electrical resistance related to the initial dimensions — 5–8%; specific heat — 15–20%; temperature — 2–3% at the level of 4000 K.

An uncontrolled change in the initial composition of carbides occurs during stationary heating of carbides due to evaporation of the components (especially intense at high temperatures). This does not allow interpreting the results obtained at stationary conditions unambiguously.

A peculiarity of heating by a microsecond current pulse is its short duration and high heating speeds. The short heating time allows preserving the initial composition of the sample, which is an advantage of this method. However, at high heating rates, a number of questions arise:

— what pressures arise in the sample?

— is it possible to consider the state of the sample homogeneous in temperature and pressure during heating?

— how will the pressure affect the measurement of the enthalpy and heat capacity of the sample?

Let's consider these questions.

Volumetric heat release occurs in each section of the specimen. Experiments performed under the same conditions on the same specimen, with analyses of different sections of the specimen surface, did not reveal a significant difference in the temperature of these sections, i.e., the temperature differences along the length of the samples did not exceed the measurement error (about 100 K at the level of 4000 K). The decrease in the temperature of the specimen surface compared to the temperature inside the sample, due to radiation losses, is negligible [33]. All this allows us to assert that the temperature distribution of the specimen along its length and cross section is homogeneous.

Experiments have shown that the most efficient design of a cell with a specimen is one in which the specimen is placed symmetrically between two dielectric plates. Due to the inertia of the plates, the heating and expansion of the specimen is accompanied by an increase in pressure in it. In addition, pressure occurs in the specimen due to the action of ponderomotor forces. Depending on the cell design, the amplitude and duration of the current pulse, and the expansion rate of the specimen, the sum of these pressures can reach tens of kilobars [20]. It is necessary to assess the level of pressures arising in experiments with carbides.

To fix the specimen in the cell, glue was used, which, after curing, formed a layer of polymethylmethacrylate (PMMA, ~ 10 μm), separating the specimen surfaces from the dielectric plates (K8 glass or silica glass). To simplify the problem, we may disregard the PMMA layer and assume that the specimen is in direct contact with the glass plates of the cell. To estimate the dynamic pressure P_d that occurs during the expansion of the specimen (in a closed volume), we use the ratio [34]

$$P_d = \gamma_2 c_2 U, \tag{1}$$

where γ_2 and c_2 are the density of the medium and the speed of sound in the medium in which the specimen is expanding, and U is the speed of movement for the specimen boundary during its expansion. We estimate this speed for a plate specimen. Assuming a specimen thickness of 0.14 mm, an average coefficient of linear expansion of zirconium carbide $\sim 7.6 \times 10^{-6}$ K^{-1} for the temperature range of 300–3300 K [12], and the heating time up to 3300 K is 3 μs ($dT/dt \sim 5 \times 10^8$ K s^{-1}), we get $U \sim 0.5$ m s^{-1}. Then, given the options for glass ($\gamma_2 \approx 2.6 \times 10^3$ kg m^{-3}, $c_2 \approx 5.8 \times 10^3$ m s^{-1} [35]), we obtain $P_d \approx 8$ MPa.

The distribution of this dynamic pressure in the specimen can be considered homogeneous if the time of propagation of the disturbance through the thickness of the specimen is sufficiently small compared to the heating time. According to calculations [36], the velocity of longitudinal waves in zirconium carbide at room temperature is ~ 8000 m s^{-1}. At 1000 K, it decreases to ~ 7000 m s^{-1}. With a specimen thickness of 140 μm, the propagation time of the disturbance will be 0.02 μs, which is significantly less than the heating time of the specimen before melting, about 3 μs, i.e., the distribution of dynamic pressure over the thickness of the specimen during heating can be considered homogeneous.

In the experiments of the authors, specimens of carbides were used in the form of thin plates with a thickness-to-width ratio of $2\delta/h \sim 0.04$ and in the form of coatings with $2\delta/h \sim (1-6) \times 10^{-4}$. The length of the specimens was 2–4 times greater than the width. To estimate the electromagnetic pressure, such specimens can be considered infinite in two directions and the pressure change considered only along the thickness of the specimen. The distribution of the electromagnetic pressure P_e (pinch effect) over the thickness

of an infinite plate with a stationary current is described by the formula [37]

$$P_e(z) = \frac{1}{4}\mu\mu_0 j^2(\delta^2 - z^2)\,, \qquad (2)$$

where j is the current density, μ is the magnetic permeability (for carbides $\mu \approx 1$), μ_0 is the magnetic constant, δ is half the thickness of the sample, and z is the distance from the specimen axis. For samples of carbides in the form of plates (ZrC, HfC), the amplitude of the current pulse was ~ 25 kA, the thickness of the plates was 0.14 mm, the maximum current density was $\sim 5 \times 10^{10}$ A m^{-2}, and the maximum pinch pressure on the specimen axis was ~ 4 MPa. The thickness of thin coatings is about 100 times less than the thickness of plate specimens, i.e., at the same current density, the pressure in these specimens is negligible ($\sim 10^4$ times less than in the case of plates).

Summing up, we see that, in our experiments with plate specimens, the pressure on the specimen surface was ~ 8 MPa, and the maximum pressure on the specimen axis reached ~ 12 MPa (for thin coatings, the total pressure is negligible).

These estimates are consistent with those obtained by another method for plate specimens of zirconium nitride [37]. It is also shown that the difference between the enthalpy of the specimen H from the energy E Joule heating at different pressures P can be calculated according to the formula

$$\frac{H-E}{E} = \frac{V_0 P}{E}\left[1 + \beta(T - T_0)\right]\left(1 - \frac{P}{2K_T}\right), \qquad (3)$$

where V_0 is the specific volume of the specimen at the initial (room) conditions, β is the coefficient of the average volumetric thermal expansion for the temperature range of $T - T_0$, and K_T is the isothermal bulk modulus. The energy of Joule heating is equal to

$$E = \frac{1}{m}\int_0^t IU\,\mathrm{d}t\,, \qquad (4)$$

where m is the mass of the specimen, and I, U are the current through the specimen and the active component of the voltage in the specimen: $U = u - L\,\mathrm{d}I/\mathrm{d}t$, where u is the voltage on the specimen, and L is the inductance of the specimen. For zirconium carbide at 3300 K, energy $E \approx 2.2 \times 10^6$ J kg^{-1}. According to [13], for carbide zirconium, $V_0 \approx 1.5 \times 10^{-4}$ m^3 kg^{-1} (density $\approx 6.6 \times 10^3$ kg m^{-3}) and, at a temperature of 3300 K, $\beta = 3\alpha \approx 3 \times (7.6 \times 10^{-6})$ K^{-1}; $K_T \approx 170$ GPa; (α — coefficient of linear thermal expansion).

An estimation using formula (3) shows that, at our pressures (11 MPa), the difference between the enthalpy and the input energy E is negligible, $\sim 0.1\%$, i.e., energy E in our experiments (with the specified specimen sizes and a heating duration of 3–5 μs) is equal to the enthalpy, provided that the thermal losses of the specimen are small.

Under our conditions, the specific heat is measured at constant pressure C_p, because, according to estimates [28], a change in pressure within 1–100 MPa leads to a change in the specific heat within 1%, which is significantly less than the error of measuring the specific heat.

It is also necessary to consider what happens to the layers of glue covering the specimen. During heating, PMMA melts at the boundary of the specimen (at about 200 K), and its decomposition and evaporation occur at ~ 1000 K [38]. During the heating of the specimen, $\tau \approx 3$ μs, the depth of the heated PMMA layer is $l \sim \sqrt{a\tau} \approx 0.5$ μm, ($a \approx 10^{-7}$ m^2 s^{-1} is the thermal conductivity estimated from the data [35] on the thermal conductivity, specific heat, and density of PMMA). Thus, during heating, the specimen is separated from the main PMMA layer by low-heat conducting thin gaseous layers. The thickness of the PMMA layer varies slightly. The preservation of this layer is observed on fragments of cells after the experiment.

For our specimens, the ratio of the specimen thickness to the grain size was at least 10. Here, we assume that the results of the study will not change with increasing specimen thickness if this ratio is ~ 10 or higher.

3. Study of zirconium carbide ZrC

The thermodynamic properties of carbides of transition metals of group IV (Ti, Zr, Hf) are due to the nature of the elements forming them and clearly reflect the change in the nature and strength of the chemical bonds in the studied compounds. Monocarbides of the listed metals, the most interesting in practical terms, are referred to as metal-like (covalent-metallic) carbides. The chemical bond in them is due to the interactions of $M-C$ and $M-M$, reflecting the mutual influence of covalent and metallic contributions.

In [39], special attention is paid to the analysis of experimental and theoretical studies devoted to the nature of chemical bonds and structural defects that directly affect the thermophysical, electrical, mechanical, and other properties of zirconium carbide. The stronger the bond in a chemical compound, the lower its specific heat should be. An analysis of the specific heat isotherms for five zirconium carbides ZrC_x ($x = 0.65-0.99$) in the homogeneity region showed that, with a decrease in the defectiveness of the carbon sublattice, the specific heat decreases almost linearly. This can be considered a consequence of the increase in the total strength of the chemical bond ($M-C$) in zirconium carbide from the lower to the upper boundary of the homogeneity region.

The observed regularity is confirmed by the change in the strength of the $M-C$ bond ($M = Ti, Zr, Hf$) during the transition from titanium carbide to hafnium carbide. An increase in the number of binding electrons enhances the interaction of $M-C$, which leads to a decrease in the specific heat in the series titanium carbide–zirconium carbide–hafnium carbide.

The most studied carbide among refractory carbides of metals of groups IV and V (Zr, Hf, Ta) is zirconium carbide. A large number of original and review papers have been devoted to the study of the thermodynamic properties of ZrC_x in the field of homogeneity, as well as the Zr–C system. The results of numerous measurements of the specific heat and enthalpy increments of crystalline zirconium carbide are presented in [40–51].

The thermodynamic properties of the liquid phase, such as the temperature dependences of the enthalpy and specific heat, and the melting enthalpy have been studied relatively recently. Prior to the appearance of experimental data, either the liquid phase of ZrC_x was not considered, or the estimated characteristics were given. The specific heat of $ZrC_{0.95}$ in the solid phase near the melting point and in the liquid state up to 5000 K was studied in [25, 26, 28].

As a result of numerical processing of experimental data, an equation approximating the temperature dependence of the specific heat of liquid zirconium carbide $ZrC_{0.95}$ on the

melting temperature of 3850 K to 5000 K was presented for the first time [31].

Based on a critical analysis of the entire array of experimental data on the thermodynamic properties of solid and liquid zirconium carbide, with a composition close to stoichiometric, equations are obtained and thermodynamic functions (specific heat, entropy, enthalpy increments and reduced Gibbs energy) for $ZrC_{0.95–0.99}$ in the temperature range of 100–5000 K are calculated [39, 52]. The obtained results are included in the database of the IVTANTERMO software package.

The processing of high-temperature experimental data on specific heat and enthalpy, performed in [39, 52], indicates a smooth but more intensive increase in the specific heat of ZrC_x above $\sim$ 2200 K. The authors of the above calorimetric studies themselves explain this phenomenon by the formation and increase in the concentration of equilibrium vacancies. On the basis of these data alone, it is difficult to draw a final conclusion about which sublattice (metal or carbon) forms thermal vacancies. The authors of study [53], comparing experimental data on the enthalpy of titanium, zirconium, and niobium carbides of various compositions in the field of homogeneity, came to the conclusion that the formation of vacancies occurs in the carbon sublattice. This is confirmed by the following facts: (1) with a change in the carbon concentration in the carbide, the heat of vacancy formation also changes, although the metal concentration remains constant; (2) the heat of vacancy formation for carbides of different transition metals (Ti, Zr, Nb) with equal defects are close to each other, that is, they do not depend on the nature of the metal.

In review [39], special attention is paid to the analysis of experimental and theoretical studies [53–64] devoted to the nature of structural defects and chemical bonds that directly affect the thermophysical, electrical, mechanical, and other properties of transition metal carbides for group IV (Ti, Zr, Hf). It is concluded that the thermodynamic properties of these carbides are due to the nature of the elements forming them and clearly reflect the change in the nature and strength of the chemical bond in the studied compounds.

The violation of the ideal crystal structure of transition metal carbides due to the formation of equilibrium thermal vacancies correlates with the temperature dependences of specific heat, enthalpy, and electrical and thermal conductivity. As numerous studies of the temperature dependence of the electrical resistance of carbides have shown, the resistance increases with an increase in the vacancy concentration, since defects in the crystal lattice lead to additional scattering of conduction electrons [60]. The influence of structural defects of zirconium, titanium, and silicon carbides on their thermophysical properties, in particular, on thermal conductivity, was studied in [64]. Theoretical calculations of the formation energies of various defects have confirmed that vacancies in the carbon sublattice are the dominant defects in ZrC_x and TiC_x carbides. Analyses of the contributions made by different scattering mechanisms at high temperatures, according to [49], allows us to assume that the main contribution is due to the scattering of electrons on the defects of the crystal lattice.

It should be noted that, in addition to structural defects, the properties of transition metal carbides, in particular, mechanical properties, are affected by such imperfections of the crystal lattice as dislocations, texture, and porosity of the specimens.

Despite numerous studies of zirconium carbide, the phase diagram for it continues to be refined [31]. In particular, there is no generally accepted value of the liquidus temperature. There are no experimental data for the region of the phase diagram with a high carbon content (for hypereutectic compositions). Until recently, data on its thermophysical properties in the solid phase before melting and in the liquid phase were obtained only by calculations. The use of the current pulse heating method made it possible to advance in solving these problems and obtain experimental data in previously inaccessible areas [25].

This method allows us to obtain a thermogram of heating and temperature dependences of various properties (enthalpy, specificheat, electrical resistance), which together allow us to clearly record the beginning and end of melting, to obtain a melting plateau (area). Thus, it becomes possible to determine the solidus, liquidus, and eutectic temperatures and to measure the heat of melting, i.e., obtain data on the phase diagram of a binary system.

In this connection, a question arises about the applicability of the data obtained by the microseconds heating method to phase diagrams, which are constructed on the basis of experimental data obtained under equilibrium conditions by stationary methods. We are talking about determining the values of T_{sol}, T_{liq}, T_{eut}. Previously, it was experimentally shown for metals (for tantalum) [17] that, when a sample is heated at a rate of $\sim 10^8$ K s^{-1}, the melting point remains the same as in the case of stationary heating. In [24], the experimentally obtained eutectic temperature T_{eut} in the ZrC–C system coincided with the value of this temperature measured by stationary methods. It is also shown that, during the melting of the eutectic under conditions of rapid heating, the system was in local thermodynamic equilibrium. The coincidence of the measured temperatures T_{sol}, T_{liq}, T_{eut} for various specimens of zirconium carbide with the data given in the literature indicates the applicability of the microsecond heating method for the study of phase diagrams of carbides.

Specimens of zirconium carbide ZrC + C (C/Zr $\approx$ 3.8) with a large excess of free carbon [24] and specimens of $ZrC_{0.95}$ [25] were studied. The ZrC + C specimens (C/Zr $\approx$ 3.8) were made in the form of a mirror thin layer deposited on a silica glass substrate by magnetron sputtering. The $ZrC_{0.95}$ specimens (designated as ZrC) were cut off from a block sintered from carbide powder by spark plasma sintering (SPS). Table 1 shows the compositions of the studied specimens. The analysis showed that, in both cases, the specimens consist of zirconium carbide with a cubic lattice. The thickness of the sprayed specimens was 4.9 μm, and the sintered one was 50–100 μm. The width and length of the first were 8 × 15 mm and the density was 4.3 g cm^{-3}; for the second, 5 × 15 mm and 6.57 g cm^{-3}.

To measure the temperature of the sprayed specimens, the radiation of a flat surface of the specimen and the radiation of a wedge-shaped blackbody model (MST) composed of flat specimens were used (Fig. 1a). The estimated effective emissivity of such a model was 0.9–0.95 [33].

The use of the blackbody model (BBM) made it possible to measure the true temperature of the specimens, as well as to measure the spectral emissivity of carbide at a wavelength of 856 nm in the solid phase at high temperatures. The blackbody model, shown in Fig. 1a, consisted of two substrates with sprayed layers forming a mirror inner surface of a wedge-shaped cavity. An electric current was passed along the plates along their entire width. The pyrometer focused on the upper

Table 1. Composition of specimens.

Carbide	Zr	C	N	O	Al	As	Hf	Summary, at.%
ZrC + C, at.%	17.88	67.69	8.13	5.98	0.16	0.17	—	100.01
ZrC, at.%	47.4	45.0	3.4	3	—	—	0.4	99.2

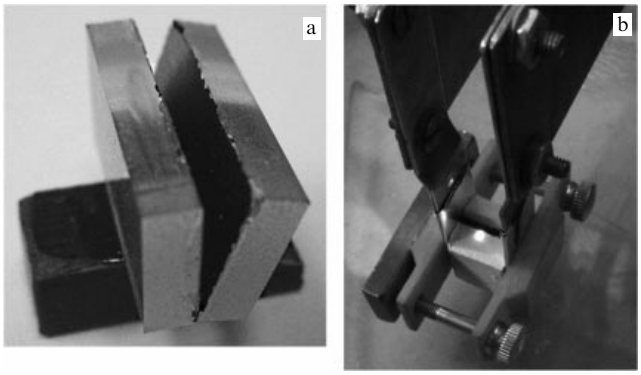

Figure 1. (a) Wedge-shaped model of a blackbody model (BBM) consisting of two glass plates (on a stand) with conductive carbide (ZrC + C) sprayed on the inner flat surfaces. (b) Focusing of the radiation spot on the BBM. Light spot (offset relative to the slit) shows the size of the emitting region. Cell is clamped at the ends by current-carrying electrodes through thin indium gaskets.

part of the cavity (Fig. 1b). It should be noted that, to rule out a shunt discharge along the inner surface of the BBM, we were forced to fill the model cavity with degassed (boiled) water. As it turned out, the absorption in the water layer was small, and we were able to reliably fix the beginning of the melting region.

In the case of using specimens in the form of plates clamped between glasses, the occurrence of a discharge is completely excluded. But, at the same time, to determine the temperature of flat ZrC specimens, we had to use known data on the normal spectral emissivity of zirconium carbide.

The experimental results are the temperatures of the beginning and end of melting, the heat of melting, as well as the temperature dependences of the specific energy dissipated in the specimen (enthalpy), the specific heat, and the electrical resistance related to the initial dimensions of the specimen.

Note here that, for ZrC, the specific heat from 1600 K to 2400 K was measured in [50] under stationary heating, but followed by pulse heating. A more detailed comparison of the obtained results with data in the literature is presented in [24, 25].

The heat of melting ΔE during pulsed current heating was determined as the energy difference at the end and beginning of melting. In the case of sprayed specimens, this difference was taken into account in that the thermal losses for heating the substrate are approximately the same for the beginning and the end of melting (this is the main type of loss). We obtained $\Delta E = 3.2$ kJ g^{-1} for (ZrC + C). For sintered specimens, the Joule energy difference was also taken into account, and we obtained $\Delta E = 1.1$ kJ g^{-1}, a value consistent with data in the literature for sintered carbide.

Taking into account the smallness of heat losses, the specific heat is determined from the dependence $E(T)$ as $C_p(T) = \Delta E/\Delta T$ ($\Delta T \approx 150-250$ K) [28]. The temperature dependences of the specific heat are shown in Fig. 2a and 2b. The arrows in the figures show the beginning and end of melting, while the sections of the curves between the arrows are illustrative — they show the result of applying calculation algorithm [28] to the melting region for which the specific heat is infinite.

The specific heat for ZrC + C specimens is ≈ 0.8 J g^{-1} K^{-1} in the temperature range of 2200–2800 K. The estimate according to the Kopp–Neumann rule for this composition assumes that the specimen consists of 75 mol.% stoichiometric ZrC, and 25 mol.% C gives a close value of the specific heat of ≈ 1 J g^{-1} K^{-1} (data for ZrC and C are taken from [65]). The specific heat for ZrC specimens (sintered) is ≈ 1.0 J g^{-1} K^{-1} in the temperature range of 2500–3000 K, which is 25–30% higher than the literature data (this is possible due to the presence of initial impurities and defects). The values of the specific heat of these two types of specimens in the liquid phase approximately coincide with each other and coincide with the calculated literature data.

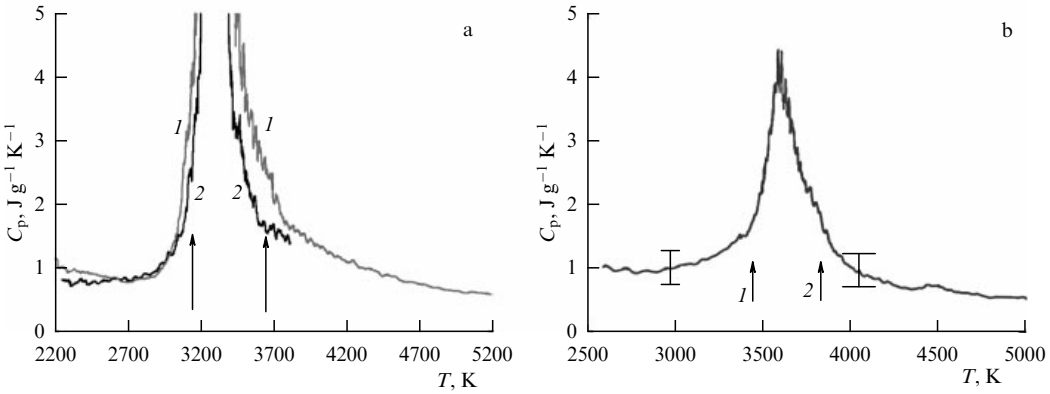

Figure 2. (a) Specific heat of ZrC + C specimens. Curve *1* is obtained with a clamped specimen, and curve *2* is obtained with a blackbody model (BBM). Arrows show the beginning (3150 K — left arrow) and the end (3640 K — right arrow) of the phase transition according to radiation registration [24]. (b) Specific heat for ZrC specimen (sintered). Arrows indicate the beginning (3450 K) and the end (3850 K) of melting. Measurement errors are shown by horizontal and vertical dashes [25]. Specific heat peaks are the result of a formal calculation of C_p in the melting temperature region close to a constant value [28].

A characteristic feature of the $C_p(T)$ dependences is a sharp increase in the specific heat (300–400 K before melting) and a sharp decrease after melting. The same change in the specific heat during rapid heating is observed during the melting of refractory metals [19, 22]. A possible explanation for this behavior for $C_p(T)$ is the assumption that nonequilibrium paired Frenkel defects are formed immediately before melting [66] (due to the impossibility of saturation of the lattice with equilibrium vacancies for a short experimental time) and then quickly disappear after melting.

It should be noted that almost all stationary data on the specific heat for carbides are obtained as a result of differentiation of the temperature dependence of the enthalpy measured by the mixing method. Since it is difficult to estimate the error value of these data, additional pulse heating is sometimes used.

3.1 Experiments with sprayed ZrC + C carbide

A carbide coating was applied to substrates made of K-8 glass by magnetron sputtering. The dimensions of the coating were $0.0049 \times 8 \times 15$ mm. The surface of the coating had a silver-gray color and a mirror reflection. Microstructural analysis indicates that the surface is composed of grains 15–60 nm in dimensions, combined into agglomerates with a size of 100–500 nm. X-ray diffraction analysis showed that the coating consists of ZrC, and the peaks on the diffractogram corresponding to the ZrC structure were greatly widened, which indicated the presence of mechanical stresses in the film. Elemental analysis determined that the specimens consist of carbon and zirconium in the ratio C/Zr ≈ 3.8 and also found the presence of nitrogen admixture — 8.1 at.% — and oxygen — 6 at.% The nitride and oxide phases of zirconium were not detected separately in the specimens. The presence of excess carbon in the specimens led to a decrease in its density compared to the density of stoichiometric monocarbide ZrC: 4.3 g cm^{-3} instead of 6.6 g cm^{-3}.

The studies were carried out with three types of specimens: flat ones with a free surface, flat ones covered with a transparent substrate ('sandwich' type specimens, clamped specimens), and those in the form of a wedge-shaped blackbody model BBM (Fig. 1a). To rule out a shunt discharge on the specimen surface, in the first and last cases, the experiments were carried out in water, and in the second case, in air.

To measure the temperature, the thermal radiation of the specimens at a wavelength of $\lambda = 856$ nm was used. To measure the true temperature, a wedge-shaped blackbody model was used. It consisted of two substrates that were folded together, forming a wedge with an angle of $\theta = 14^\circ$ between the sprayed layers (Fig. 1a). The blackbody model was clamped to the electrodes with insulating plates using connecting screws (Fig. 1b). Such a model withstands rapid heating and continues to exist without changing its shape in the liquid phase for a time (several microseconds) sufficient to measure the temperature. The measurement of the specimen temperature in the form of a wedge-shaped blackbody model is described in detail in [33].

The effective emissivity $\varepsilon_{\text{eff},\lambda}$ of such a model with a mirror reflection of its walls can be calculated by the formula

$$\varepsilon_{\text{eff},\lambda} = 1 - (1 - \varepsilon_{\text{n},\lambda})^{\pi/\theta}, \tag{5}$$

where $\varepsilon_{\text{n},\lambda}$ is the normal spectral emissivity of the walls and θ is the angle of the wedge.

According to [67], $\varepsilon_{\text{n},\lambda}$ for zirconium carbide is 0.562 for a wavelength of 856 nm at a temperature of 2900 K (obtained by interpolation of tabular data [67]).

We assumed $\varepsilon_{\text{n},\lambda} = 0.6$ for the solid and liquid phases of the specimens (see below). In this case, formula (5) gives a value greater than 0.99. In the other extreme case of diffuse reflection of walls, $\varepsilon_{\text{eff},\lambda}$ can be estimated using the expression

$$\varepsilon_{\text{eff},\lambda} = \frac{\varepsilon_{\text{n},\lambda}}{\varepsilon_{\text{n},\lambda} + (1 - \varepsilon_{\text{n},\lambda})\sin(\theta/2)}, \tag{6}$$

which gives $\varepsilon_{\text{eff},\lambda} = 0.92$ for $\varepsilon_{\text{n},\lambda} = 0.6$.

To calculate the true temperature, the value $\varepsilon_{\text{eff},\lambda} = 0.95$ (average value between 0.92 and 0.99) was taken. When the specimen turns into a liquid, its reflection becomes only a mirror, but in this case, the value $\varepsilon_{\text{eff},\lambda} = 0.95$ was used.

In measuring the temperature of specimens covered with glass, the absorption of the upper cover glass was taken into account, and for all specimens (including the blackbody model), the absorption of the protective glass, located in front of the pyrometer lens, was taken into account. In calculating the temperature of flat specimens and the blackbody model, the reflection of radiation from the water–air boundary was taken into account. The absorption of radiation at a wavelength of 856 nm in a water layer (equal to the depth of the blackbody cavity of 8 mm) was estimated as insignificant.

The wedge-shaped blackbody model was successfully used to measure the true temperature in experimental studies [68, 69] for the metals Zr, Hf and in [70] for carbon. The application of such a model is also described in detail in book [22]. Experimental waveforms for one of the ZrC + C specimens are shown in Fig. 3a.

During pulsed heating, the specific Joule energy released in the sample at time t will be equal to

$$E = \frac{1}{m}\int_0^t i(t)U(t)\,\mathrm{d}t, \tag{7}$$

where m is the mass of the ZrC + C; $i(t)$ layer, the current through the specimen, and $U(t)$ is the voltage drop along the specimen, taking into account the correction for its inductance. To calculate E(t), the waveforms shown in Fig. 3a, presented in digital form, are used.

To understand the heating features of thin-film sprayed specimens, it is of interest to compare the results obtained with specimens in the form of the BBM and with clamped specimens. Figure 3b shows the dependences of the temperature for specimens in these two cases against the energy introduced.

The obtained dependences show that the melting start temperatures of 3120 K (clamped specimen) and 3150 K (blackbody construction) correspond to the joule energy $E = 2.65$ kJ g^{-1}. Taking into account the losses to the substrate, the enthalpy of the specimen is 2.35 kJ g^{-1}. The Joule energy of the beginning of the phase transition for the blackbody model coincides with the data for a clamped flat specimen (sandwich). But at the end of the melting, these values do not match. For a sandwich specimen, a higher specific joule energy is recorded at the end of the phase transition (5.85 kJ g^{-1} instead of 5.2 kJ g^{-1} for a blackbody). Taking into account the losses to the substrate, the corresponding enthalpy is 5.55 and 4.9 kJ g^{-1}. This indicates that the blackbody model (without limiting the specimen from the surface with a solid insulating wall) begins to break

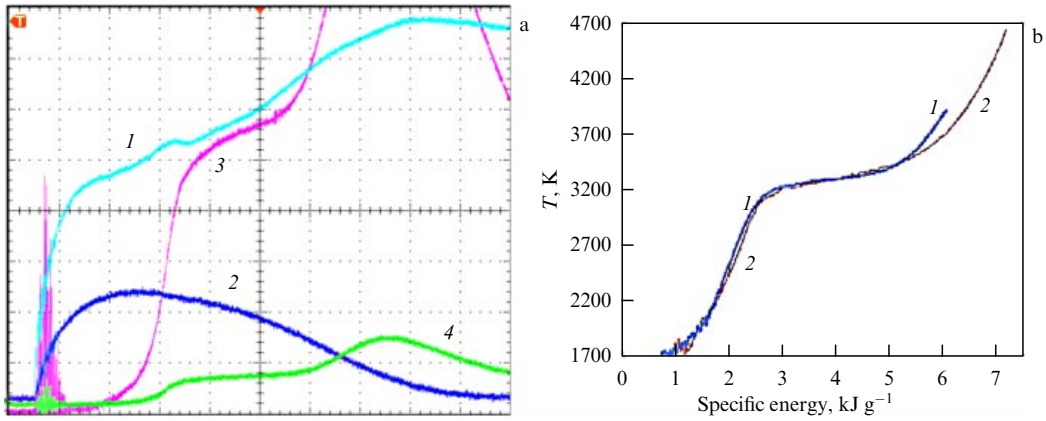

Figure 3. (a) Waveforms for the blackbody model (ZrC + C). Melting region looks like an inclined plateau in curve *3*. *1* — voltage; *2* — current pulse; *3* — radiation from a wedge-shaped blackbody model (high sensitivity); *4* — the same as in *3*, but with less sensitivity. Full-screen sweep — 10 μs. (b) Comparison of the results of measuring the temperature for ZrC + C, depending on the energy introduced, using the blackbody (curve *1*) and the clamped specimen (curve *2*).

away from the glass and collapse even before the end of the phase transition. Therefore, a specimen in a 'sandwich' type cell, that is, in a limited volume, allows one to study the substance in the melting region and in the liquid state at significantly higher temperatures. In this regard, measurements of the temperature of ZrC + C at the time of completion of the phase transition were carried out using clamped specimens instead of a blackbody model. The blackbody model was used only to determine the temperature of the beginning of the phase transition and to obtain the spectral emissivity of ZrC + C in the solid phase for the phase transition region.

Thus, for ZrC + C film specimens, experiments show the following results. The phase transition (melting) begins at 3150 K with an enthalpy of 2.35 kJ g^{-1}. The resistivity at this point is 700 μΩ cm. The temperature at the end of the phase transition is 3640 K at the enthalpy of 5.55 kJ g^{-1}, and the resistivity is slightly higher — 900 μΩ cm. The phase transition occurs in the temperature range of 3150–3640 K. The heat of the phase transition is 5.55 − 2.35 = 3.2 kJ g^{-1}.

As a result of the experiments conducted, it can be concluded that the method of rapid current heating allows us to study the phase diagram, not only to fix the lines of the eutectic isotherm, solidus, and liquidus during the phase transition for the ZrC + C system, but also to measure other thermophysical properties. Judging by the published literature, the region of the phase diagram with high carbon content is the least studied. It is known in [71–73] that, at low external pressure (below 120 bar), carbon sublimates at high temperatures not only from the surface but also into internal pores.

This creates additional difficulties in the study of carbon and ZrC + C specimens (with a high C content). It was shown in [23] that a thin film of ZrC + C (not covered with glass from above) breaks off from the substrate immediately before the end of melting. The use of a cell with a specimen clamped between the plates is a way to measure the properties of carbides with a high carbon content at the highest temperatures. This design also prevents a loss of carbon by the specimen, i.e., conditions are created under which the composition of the specimen does not change during heating.

Laser pulse heating is also used for the study of ZrC + C at high temperatures. In particular, the liquid phase of the eutectic was studied in [74] for the composition of the compound $0.7 \leqslant C/Zr \leqslant 2.61$. A high-speed spectropyrometer was developed for the spectral range $0.550 \leqslant \lambda \leqslant 0.900$ μm. The normal spectral emissivity ($\varepsilon_{n,\lambda}$) in the solid state turned out to be equal to 0.6 at a wavelength of 650 nm, which corresponds to other literature data. For the first time, the radiation characteristics in the near-infrared zone for the liquid state at an increased carbon concentration were studied. A significant increase in $\varepsilon_{n,\lambda}$ was observed with an increase in the carbon content in the compound.

3.2 Experiments with sintered ZrC carbide (C/Zr = 0.95)

A target made of zirconium carbide in the form of a disk with a diameter of about 40 mm and a thickness of 5 mm was made by the spark plasma sintering method (SPS method) at the All-Russian Institute of Aviation Materials (VIAM). ZrC powder with an initial grain size of less than 40 μm was used. Sintering mode: temperature — 2300 K; pressure — 35 MPa; holding time — 30 min. The target was cut into plates (width of 5 mm, length of 15 mm, thickness of about 250 μm) using a diamond disc. Then, the obtained plates were polished manually on diamond bars until a thickness of 50–100 μm was obtained. The specimen surface was processed on a diamond bar with a grain size of 7 μm. Similar methods were used by us earlier [75]. The carbide density was determined by weighing a part of the initial disk on a GR-202 electronic scale (A&D Corporation, Tokyo, Japan) and determining its geometric dimensions. The density was found to be equal to 6.57 g cm^{-3}. The formula for calculating the ZrC_x density is given in review [61]:

$$d = 6.05 + 0.24x + 0.32x^2 \quad (\text{g cm}^{-3}) . \tag{8}$$

For our case, $x = C/Zr = 0.95$ ($ZrC_{0.95}$), which gives a density equal to 6.567 g cm^{-3}. The coincidence of the measured and calculated density indicates a very low porosity of the specimens. The specimens had the following composition: (average data for three points, at.%): C — 45.0; Zr — 47.4; Hf — 0.4; N — 3.4; O — 3. The remaining impurities were Fe, Ni, Na, Al.

The phase composition of the specimen was studied by X-ray diffraction analysis using the DRON-2 apparatus (CuK_α — radiation) according to the standard method. The

analysis showed that the dominant phase in the material is zirconium carbide ZrC, which has a crystal lattice parameter of 0.4694 ± 0.0001 nm.

The specimen was placed between two dielectric plates (glass, silica-glass), the length of which was equal to the length of the specimen, and glued to one of them. Radiation from the free surface of the specimen was recorded through the second plate. On the side surfaces of these plates, plates made of insulating materials were glued — textolite, glass — which serve to fix such a cell with a specimen. The cell was clamped in the current leads through soft indium pads, which provided electrical contact with the fragile specimen. The experiments were carried out in the air.

The pressure in the heated sample increases due to the inertia of the outer plates. In addition, there is a pressure in the specimen caused by the action of ponderomotive forces and the inertia of the material of the specimen itself. The sum of these pressures can reach several ten kilobars [20], depending on the cell design, the amplitude and duration of the current pulse, and the expansion rate of the specimen.

However, in experiments with ZrC plates, the pressure was much lower. An estimate of its value (7–11 MPa) is given in Section 2. It is shown in [76] that, at such a pressure level, the introduced energy is almost equal to the enthalpy, and an estimate of the pressure level at which this ratio is violated is given.

The inertial effect in the substance itself and the pinch effect give an inhomogeneous pressure distribution over the specimen. It was also shown in [76] that only the inertial effect in the environment (when the expanding plate is limited by the outer wall) provides a uniform pressure in the specimen.

The temperature was measured by radiation from the flat surface of the specimen using a high-speed pyrometer based on the PDA-10A photodetector (Thorlabs). The relatively large thickness of the specimens did not allow the use of a wedge-shaped blackbody model made up of carbide plates, since the installation power was insufficient to heat such a model to melting. The optical schematic of the pyrometer is shown in Fig. 4. Before the pulse experiment, the pyrometer was calibrated using an SI-10-300 temperature tungsten lamp at a temperature of 2515 K. The measurements were carried out at a wavelength of 856 nm. The surface temperature of the carbide specimen was calculated using formula (9):

$$T = \frac{C_2}{\lambda \ln\left[U_0 \varepsilon_{\mathrm{n},\lambda} \tau_\lambda \left(\exp\left(C_2/\lambda T_0\right) - 1\right)/U \varepsilon^0_{\mathrm{n},\lambda} \tau^0_\lambda + 1\right]}, \qquad (9)$$

where C_2 is the constant in the Planck formula; U_0, U are the pyrometer signal during calibration and the signal from the sample; $\varepsilon_{\mathrm{n},\lambda}$, $\varepsilon^0_{\mathrm{n},\lambda}$ are the normal spectral emissivity of the surface for carbide and for a tungsten strip of the Si-10-300 lamp; $\tau_\lambda = \Pi\tau_{i\lambda}$ is the total transmittance of the top plate of the cell ($\tau_{1\lambda}$) and safety glass ($\tau_{2\lambda}$) elements, which are removed during calibration of the pyrometer; $\tau^0_\lambda \approx 0.92$ is the transmittance of the window for a temperature lamp; and $T_0 = 2515$ K is the temperature of the tungsten ribbon for SI-10-300. The transmission coefficient $\tau_{i\lambda}$ was measured with a Shimadzu UV-240 spectrophotometer (Shimadzu) at a wavelength of 856 nm.

Measuring the temperature of specimens requires knowledge of the emissivity of carbide in the solid and liquid phases. The normal spectral emissivity for the wavelength $\lambda = 856$ nm was chosen after reviewing the literature data in [24, 67, 77, 74]. For the solid phase of ZrC, obtained were 0.5 for 3000 K [24, 77]; 0.563 for 2900 K [67]; 0.581 for 3155 K [74]. In a study of sintered zirconium carbide ZrC, we used the value $\varepsilon_{\mathrm{n},\lambda} = 0.6$ for both the solid and liquid phases.

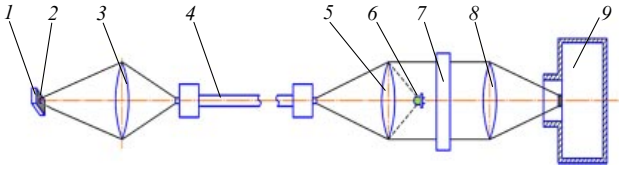

Figure 4. Radiation detection schematic [75]: *1* — substrate; *2* — specimen; *3* — focusing lens; *4* — light guide; *5* — collimating lens; *6* — LED (introduced at the time of focusing on the specimen surface); *7* — interference filter ($\lambda = 856$ nm; $\Delta\lambda = 11.5$ nm); *8* — focusing lens; *9* — high-speed PDA-10A photodetector (Thorlabs).

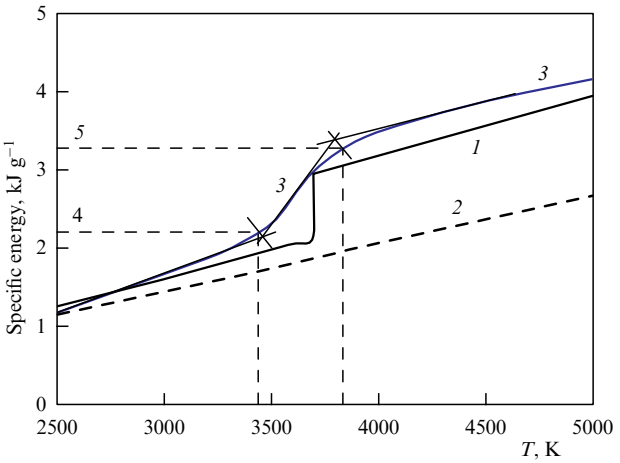

Figure 5. Dependence of Joule heating energy (enthalpy) on the temperature for ZrC. Comparison of experimental results with calculated enthalpy data. *1* — Calculated data [65]; *2* — Calculated data [78]. No phase transition is shown; *3* — this experimental study; *4* — temperature at the beginning for the phase transition $T_{\mathrm{sol}} \approx 3450$ K ($E_1 = 2.2$ kJ g^{-1}); *5* — temperature at the end for the phase transition $T_{\mathrm{liq}} \approx 3850$ K ($E_2 = 3.3$ kJ g^{-1}). Heat of melting is equal to $E_2 - E_1 = 1.1$ kJ g^{-1}. Temperature measurement error in the melting region is ±80 K.

The result of an experiment with one of the specimens and a comparison with the calculated data are shown in Fig. 5. In the calculations in [65], it is assumed that the melting of carbide occurs at a strictly defined temperature of 3693 K. The phase transition is not taken into account in [78]. It follows from Fig. 5 that the experimental specific heat of the solid phase of ZrC is higher than the calculated value near the melting region (the experimental enthalpy curve is steeper). As a result, the experimental dependence in the melting region and in the liquid phase is shifted relative to the calculated curve towards higher values. However, the measured melting heat approximately coincides with the calculated value [65].

It was established in [25] that the melting of zirconium carbide ZrC (C/Zr = 0.95) occurs in the temperature range of $\sim 3450 - 3850$ K. Figure 6a shows the temperature dependence of the specific heat of this carbide in the solid and liquid phases. Our data for the solid phase, which is a direct measurement of C_{p} for a temperature step of 150–250 K, are approximately 25% higher than those from other studies (Fig. 6a, black squares — data from [43]). The specific heat of zirconium carbide in the solid phase was studied in a number of papers [43, 44, 46, 48, 50, 79]. The data obtained in these studies are consistent with each other in the range of 10–20%,

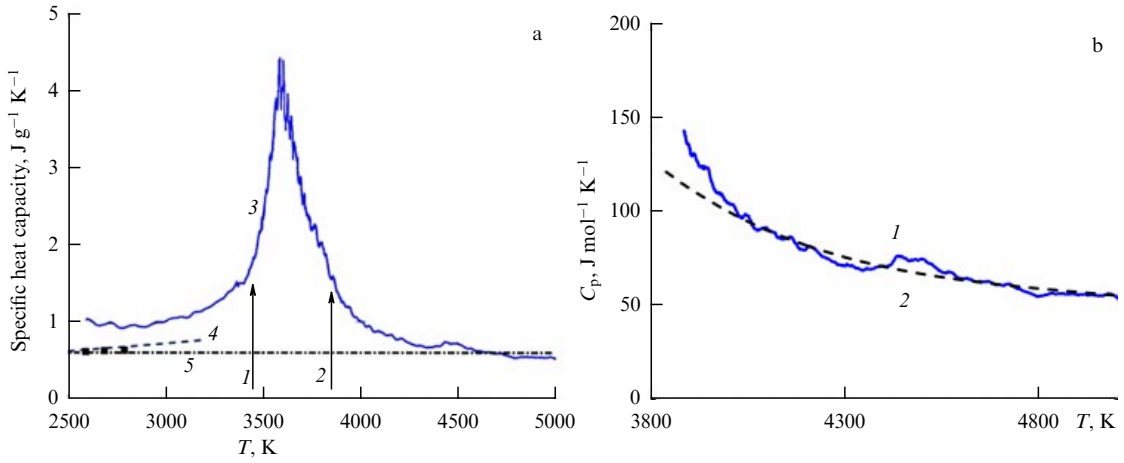

Figure 6. (a) Specific heat of sintered ZrC carbide for solid and liquid states. *1* — beginning of melting; *2* — end of melting; *3* — pulse experiment; *4* — [65]; *5* — solid state [81]. Liquid state [78]. (b) Dependence of the specific heat on temperature for liquid zirconium carbide $ZrC_{0.95}$: *1* — experimental values [25]; *2* — approximating values [31].

although they differ in the slope of temperature dependences. Among these studies, the specific heat was directly measured only in [48] and in [50]. In other studies, the specific heat was obtained by differentiating the temperature dependences of the enthalpy measured by the mixing method.

We present the result of the specific heat for zirconium carbide by the stationary pulse method. The authors of [50] give the results of measuring the specific heat of zirconium, niobium, and tantalum carbides of stoichiometric composition in the temperature range of 1600–2300 K. The test specimen was placed in a vacuum or an inert gas medium and heated to a certain constant temperature in a resistance furnace. The temperature of the specimen in the stationary state was measured by the VIMP-015 M optical pyrometer. Then, a DC electrical pulse was passed through the sample. The magnitude of this current and its duration were such that the radiant losses from the sample for the entire pulse time were a small amount ($\sim 1\%$) of the input energy. At the same time, the specimen temperature increased by only 50 K (the rate of increase in the sample temperature was 500 K s^{-1}). The temperature rise was measured by a pyrometer based on an FEU-51 photomultiplier. The error in calculating the specific heat data [50] in the studied temperature range for ZrC was 3.4%. The discrepancy between the ZrC results [50] and the majority of the literature data did not exceed 17%.

It was found in [79] and [80] that the excess of the enthalpy of zirconium carbide at temperatures above 2200 K over the values obtained by extrapolating lower-temperature data (up to 2200 K) is associated with the formation of thermal vacancies. This excess was used to calculate the energy of vacancy formation in [79, 80].

In our case of microsecond heating, the mechanism of formation of thermal equilibrium vacancies associated with their stationary diffusion in the specimen does not take place; the relaxation time of such point defects is estimated to be longer than the heating time. However, in our experiments, an increase in enthalpy is also observed, and a sharp increase in the specific heat is observed when approaching the melting point. A consistent explanation for this phenomenon is the assumption that the formation of nonequilibrium Frenkel defects (vacancy + interstitial atom) requires additional energy.

According to Fig. 6a, approximately 300 K before the start of melting (3450 K) [25], an abnormal increase in the specific heat begins. For the studied zirconium carbide in the solid phase, this effect is probably associated with the appearance of paired Frenkel defects under conditions of insufficient time for the diffusion of equilibrium vacancies. By the time of the end of melting, 3850 K, the specific heat of liquid zirconium carbide remains high (Fig. 6a, b). After the completion of melting, the specific heat decreases rapidly (within $\sim 1-2$ μs) to equilibrium values at temperatures of 4200–5000 K (Fig. 6b) [31].

The temperature dependence of the experimental values of the specific heat of $ZrC_{0.95}$ in the liquid phase obtained in [25] was approximated in [31]. Figure 6b shows the approximating curve $C_p(T)$ of liquid $ZrC_{0.95}$ in the temperature range of 3850–5000 K:

$$C_p(T) = -4250.0 + 1.16787T - 9.0 \times 10^{-5}T^2 + 1.7887 \times 10^{10}T^{-2} \quad (\text{J mol}^{-1}\ \text{K}^{-1}).$$

In [31], also provided is a brief overview of studies on the refinement of the Zr–C phase diagram: parameters of the solidus and liquidus lines, the temperature and composition of congruently melting carbide, and the eutectic temperature of ZrC–C.

The authors' result ($T_{liq} \approx 3850$ K) agrees with the data obtained by M A Sheindlin and co-authors during millisecond pulsed laser heating of zirconium carbide with a heating time of 200 ms [82]: "The congruent melting temperature is close to 3800, which is 150 K higher than the previously obtained one."

The thermophysical properties of zirconium carbide, such as enthalpy (specific energy of Joule heating), heat of melting, specific heat, and electrical resistance, were first measured in the temperature range of 2500–5000 K by the method of rapid heating by a current pulse [25]. It is established that the melting of carbide occurs in the following temperature range: solidus — 3450 K, and liquidus — 3850 K, which is close to the values presented in some equilibrium phase diagrams of the Zr–C system. This means that there is no shift of the phase transition points at heating rates up to $10^8 - 10^9$ K s^{-1} and that this method can be used to study the high-temperature behavior of complex substances.

4. Study of hafnium carbide HfC

Stationary studies of the thermophysical properties of HfC — specific heat and enthalpy — were performed in a number of papers: in [45], in the temperature range of 298–2500 K (for ZrC and HfC); in [83], enthalpy in the range of 1300–2800 K. The high-temperature enthalpy of HfC was also measured in [84] in the range of 1300–2500 K.

Recall that the first serious attempt to study in detail the properties of refractory carbides under pulsed heating was made in [85]. Temperature measurements had not yet been established, so the melting region was fixed according to the dependence of the electrical resistance on the enthalpy for ZrC and TaC carbides.

To perform a new pulse experiment, hafnium carbide specimens in the form of plates with dimensions of $0.14 \times 4 \times 15$ mm were obtained using the same technology as sintered zirconium carbide specimens. HfC powder (TU 6-09-03-361-78) with an average grain size of 40 μm was used, which was crushed to obtain a powder with an average grain size of 15 μm. The initial target in the form of a disk with a diameter of 50 and a thickness of 4 mm was made using this powder by the SPS method. Powder sintering mode: temperature rise — 100 K min^{-1}; sintering temperature — 2373 K; pressure — 45 MPa; cooling without pressure; medium-vacuum; pressure — ∼ 50 Pa. The surfaces of the HfC disk in contact with the graphite crucible during sintering were protected with molybdenum foil. After the disk was made, these surfaces were sanded to remove layers contaminated with an impurity of molybdenum. The resulting disk was cut into plates with a thickness of 0.5–0.6 mm by means of electric erosion cutting. They were then subjected to grinding to obtain a thickness of ∼ 140 μm. Finally, the surface of the specimen was ground on a diamond bar with a grain size of 5 μm. Sample thickness was ≈ 130 μm. A view of the hafnium carbide specimen in the fracture (electron microscope) is shown in Fig. 7.

The density of the sintered disk was 12.45 g cm^{-3}. According to the reference data, the X-ray density of HfC is 12.6–12.7 g cm^{-3}, which gives a porosity of HfC specimens of ≈ 1.6%.

Qualitative X-ray diffraction analysis performed in CuK_α radiation showed that only one phase is present in the specimens: HfC. It is known that the HfC lattice parameter varies from 4.606 to 4.641 Å depending on the stoichiometry. The measured lattice parameter was 4.63451 Å for the specimens studied.

X-ray spectral analysis showed that, in addition to hafnium and carbon, oxygen is included in the composition of the specimens in the form of an impurity. The specimens had a composition (at.%) of 42% C, 49% Hf, and 7% O, corresponding to the conditional formula $HfC_{0.85}$.

Views of the specimen in a glass cell and a cell mounting in current leads are shown in Fig. 8a and 8b. The carbide plate was clamped between two plates of K-8 optical glass to prevent evaporation of the carbide and to prevent surface discharge at high voltage along the specimen (the voltage on the capacitor bank is ∼ 17 kV).

Figure 9a shows oscillograms from the experiment with a specimen of hafnium carbide. The smooth bend on curve *3* is the melting region (the beginning is for 5.6 μs, the end is for 6.4 μs). Figure 9b shows the dependence of current and voltage on time for this specimen.

Let's estimate the pressure that occurs in the specimen when it is heated. We note the similarity of the properties of zirconium carbide and hafnium, the same method of obtaining specimens, and approximately the same sizes of specimens and cells with specimens. All this makes it possible to use the estimates obtained earlier in Section 2 for zirconium carbide specimens for estimates in the case of HfC specimens. For example, for HfC, the amplitude of the current pulse was ≈ 30 kA, and the pressure on the surface and in the axis of the specimen was ≈ 5 and ≈ 12 MPa, respectively.

To measure the temperature from the radiation of a flat surface for a carbide plate, it is necessary to know the normal spectral emissivity of $\varepsilon_{n,\lambda}$. In this experiment, the value $\varepsilon_{n,\lambda} = 0.6$ was assumed for HfC carbide for the solid and liquid phases in the entire temperature range. Such a value of $\varepsilon_{n,\lambda}$ for a wavelength of 0.8 μm and for a temperature of 2900 K was obtained in [86] as a result of a carefully performed experiment for a wide range of wavelengths (0.65–6 μm) in the temperature range of 2400–2900 K.

It is difficult to determine the beginning of HfC melting (as well as its end) due to smooth bends of the glow curve at the beginning and at the end of the melting region (Fig. 9a).

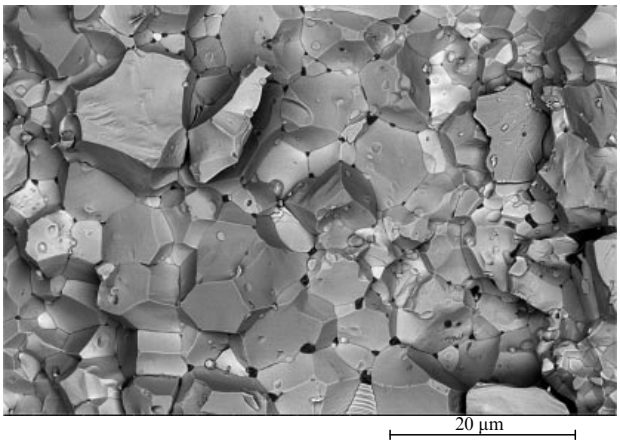

Figure 7. View of a sample of hafnium carbide (in a fracture). Thickness of the sample is ≈ 130 μm.

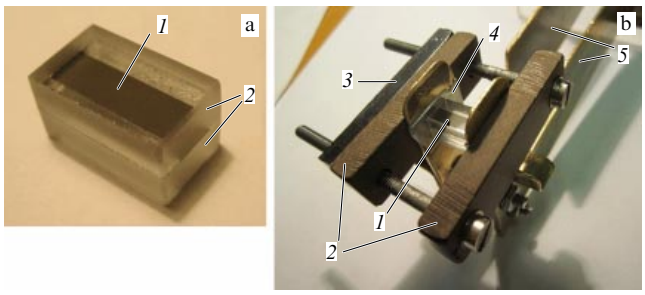

Figure 8. (a) Flat HfC specimen clamped between two plates of K8 optical glass. *1* — surface of the carbide (not covered with glue); *2* — upper and lower glasses with a thickness of 3.7 mm (their gluing did not affect the upper surface of the carbide plate). Ends of the finished cell (with glue) were polished. To eliminate shunt discharge, the slotted gaps along the specimen are filled with glue and mica strips. (b) Cell with an HfC specimen placed between the current leads (brass). *1* — carbide plate. Temperature was measured from the center of the upper plate (diameter of the radiating spot is about 1.5 mm); *2* — thick insulation plates; *3* — metal plate; *4* — thin indium foils placed between the ends of the specimen and the electrodes, which provided good electrical contact after tightening the screws; *5* — lead electrodes (brass).

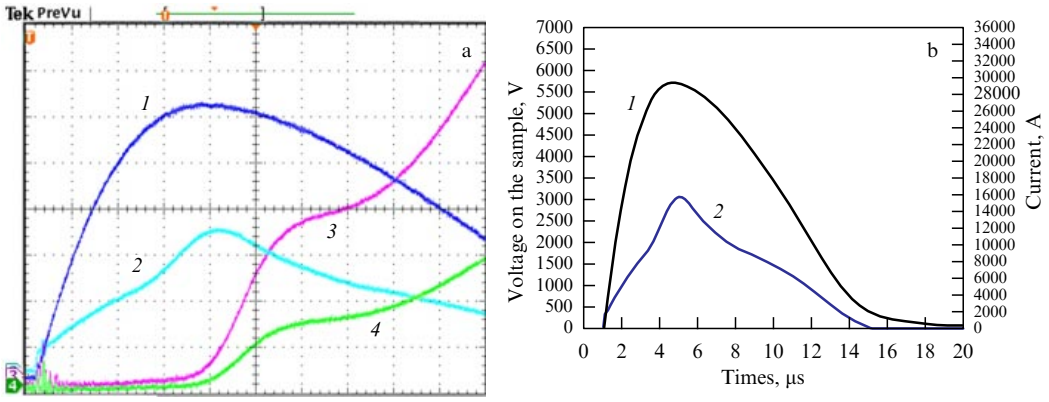

Figure 9. (a) Waveforms of a pulse experiment with one of the HfC specimens. Full screen sweep — 10 μs: *1* — current; *2* — voltage on the sample; *3* — surface radiation at a wavelength of 856 nm (high sensitivity). *4* — the same as in *3*, but with less sensitivity. (b) Current (*1*) and voltage (*2*) during pulse heating of the HfC specimen. Specimen: width 4.0 mm, length 14.64 mm, thickness 153 μm. Voltage of the capacitor bank is 17 kV (capacity — 15 μF).

The melting begins with the most defective areas — along the grain boundaries — and extends deep into the grain. Recall that the studied hafnium carbide had very large crystallites (up to 20 μm, Fig. 7). It is possible that smooth changes in the region of the phase transition (curve *3*, Fig. 9a) are associated with the large sizes of crystallites in the specimen.

The temperature of the beginning of melting was determined using a thermogram of specimen heating. The start of melting $T_{sol} \approx 4000$ K was found in the thermogram of the specimen using geometric constructions [24, 23]. These constructions were usually performed to determine the characteristic temperatures (eutectic, the beginning of melting, etc.). Indirect confirmation that this value is the melting point can be a sharp increase in fluctuations in the dependence of the electrical resistance of the specimen on time, starting from the time corresponding to this temperature, and then in the entire region of the liquid phase [30].

The difficulty of determining the moment of melting completion by the thermogram, for the dependence of the enthalpy on the temperature, was overcome as follows. The moment of completion of melting at T_{liq} is clearly visible on the dependence of the electrical resistance on time and temperature. And since the oscilloscope sweep is the same for all channels, you can easily transfer this moment to all dependences. The electrical resistance of the HfC specimen under study is shown in Fig. 10.

Now we can confidently talk about the melting range of HfC carbide: from 4000 K to 4200 K. This result can be final in the question of which carbide is more refractory: mixed carbide TaC+HfC ($T_{liq} = 4300$ K) or hafnium carbide HfC ($T_{liq} = 4200$ K). It should be noted that, for hafnium carbide, the value of $\varepsilon_{n,\lambda}$ was assumed to be equal 0.6 [86], where it was measured only for the solid phase. We also used $\varepsilon_{n,\lambda} = 0.6$ for the liquid state. For the liquid phase of HfC, the emissivity value is unknown.

It should be noted that the melting temperature of hafnium carbide was also studied under surface laser heating [87]. In this publication, its authors obtained the melting point of HfC carbide (at a carbon content of about 48 at.%): 4255 ± 30 K. In our experiment, the carbon content is 46 at.% (the melting completion temperature is 4200 ± 80 K).

Measurements of the solidus and liquidus temperatures are consistent with the phase diagram of the Hf–C system given in [10], and, as shown in [25], with the results of [87]. The

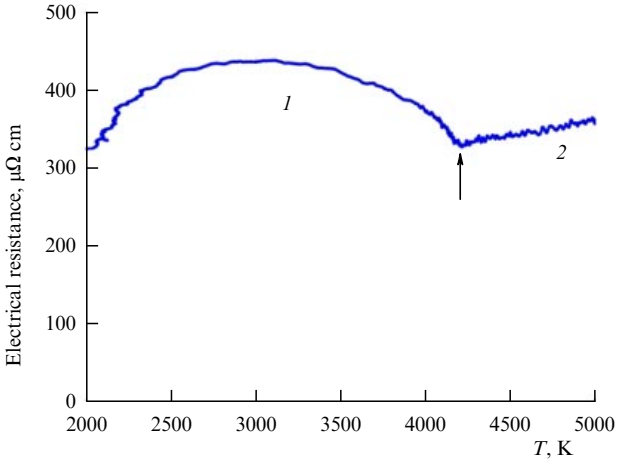

Figure 10. Electrical resistivity (referring to initial dimensions) for an HfC specimen with a thickness of 153 μm, depending on the measured temperature. *1* — solid state (including melting); *2* — liquid state. The arrow indicates the transition of the entire volume of the specimen to the liquid state, i.e., $T_{liq} = 4200$ K.

specific heat C_p for hafnium carbide (indicated for two specimens) is shown in Fig. 11.

Before the start of melting (above 3500 K), an accelerated increase in the specific heat occurs, which, in our opinion, is associated with the formation of Frenkel defects. The specific heat for rapid heating is slightly higher than for stationary heating from 2500 to 3500 K. Impurities and initial defects remain in the specimen during rapid heating. Unlike stationary heating, in which these defects and impurities can migrate and leave the specimen, in a fast process they remain in the specimen until melting. The Frenkel defects (which appeared immediately before melting) and the initial defects disappear after melting. The specific heat decreases in the liquid state to the equilibrium value for the liquid phase.

We obtain a phase transition energy (heat of melting) in our experiment of $3.4–2.6 = 0.8$ kJ g^{-1} for HfC (with an admixture of oxygen of 7 at.%). In our experiment, the carbon content is 46 at.% . For this content, we measured $T_{liq} = 4200$ K. According to our measurements in this study, $T_{sol} = 4000 \pm 80$ K. Unlike current heating, the solidus temperature during laser heating from the surface is more difficult to determine than the liquidus temperature.

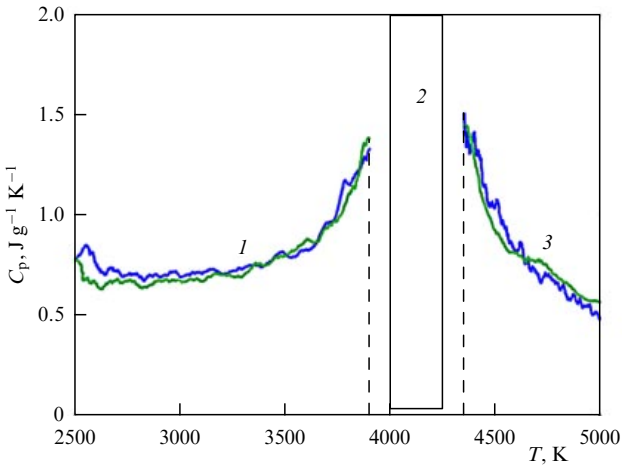

Fig. 11. Dependence of specific heat C_p of the solid and liquid states for two $HfC_{0.85}$ specimens on the temperature: *1* — solid phase; *2* — melting region; *3* — liquid phase. Dotted lines show the boundaries of the temperature intervals in which the specific heat was calculated. This was done in order not to capture the melting region when calculating the steeply increasing specific heat.

It was found in this study that the melting point of hafnium carbide (4200 ± 80 K) is slightly less than the melting point of mixed TaC–HfC carbide (4300 ± 80 K [29]). This result (obtained in [30]) for HfC (C/Hf = 0.85) coincides with the stationary measurements [88] performed using the blackbody model. In a well-known study on laser melting of carbides [89], the opposite was stated, that the melting temperature of hafnium carbide (C/Hf = 0.98, melting temperature $T_m = 4232 \pm 84$ K) is slightly higher than for TaC (C/Ta = 1.00, melting temperature $T_m = 4041 \pm 77$ K) or for mixed carbide ($Ta_{0.75}Hf_{0.25}C$, $T_m = 4178 \pm 82$ K). Note that these comparisons lie in the area of overlapping temperature measurement errors, that is, the comparison, in this case, does not make much sense. In addition, the melting temperatures of carbides obtained in various experiments (including our experiments) are mainly associated with the choice of the emissivity value, measurements of which for high temperatures are often absent.

It is necessary to note the features of fast (microseconds) electrical heating, which have become clearer after many years of using this method.

• Due to the short duration of heating (heating rate $dT/dt \sim 5 \times 10^8$ K s^{-1}), impurities and starting defects of the material (including defects of various types) are stored in the heated specimen until the transition to the liquid state. This leads to an increase in the specific heat of the solid phase in a wide temperature range before melting. Such an increase in the specific heat is absent if the source material did not contain the initial defects and impurities (for example, a quasi-monocrystal of graphite [71]);

• The short duration of the heating process limits the possibility of diffusion of equilibrium vacancies, which usually saturates the specimen volume, providing melting. Therefore, it is logical to assume that, under rapid heating, paired Frenkel defects occur (200–300 K before melting) in the entire volume, which is reflected in a sharp increase in the specific heat of the solid immediately before melting. This effect was observed for all the substances studied: metals and carbides, including quasi-crystalline graphite [71];

• The transition of the material to the liquid phase is accompanied by a sharp drop in the specific heat in the liquid phase (in the time interval of $\approx 1-2$ μs). During this time, the main defects disappear, and the specific heat of the liquid phase decreases to its equilibrium value.

Note that, for all their advantages, pure carbide ceramics, due to their high fragility, are not able to withstand thermal shock. As indicated in [90], when hafnium carbide HfC is used as a heat-protective coating in a high-temperature oxidizing flow, an oxide film is formed on the surface of the hafnium carbide. The high evaporation temperature of the hafnium oxide film makes it possible to significantly increase the heat resistance of the material as a whole. Of particular interest is the $HfC + HfO_2$ system (hafnium carbide + hafnium dioxide). Such a composition, which includes from 50% to 75% hafnium carbide HfC by volume, has a particularly high heat resistance (at more than 2300 K) with a relatively low thermal conductivity [90].

5. Physical properties of the most refractory mixed carbide $Ta_{0.8}Hf_{0.2}C$

Study [91] is devoted to the development of methods for obtaining $Ta_{0.8}Hf_{0.2}C$ and other carbides and borides for extreme application conditions. This paper contains a significant number of references to original studies on the preparation and analysis of initial carbides and their compounds. However, there are no significant papers with the results of the study of carbides at high temperatures.

In this chapter, we present the authors' experimental studies for mixed carbide up to temperatures above the melting point.

Carbide $Ta_{0.8}Hf_{0.2}C$ (the conditional formula describing the composition of the studied specimen is $Ta_{0.81}Hf_{0.19}C_{0.94}$) in the form of a thin sprayed layer (≈ 1 μm) was studied under rapid heating (5 μs, heating rate $dT/dt \sim 5 \times 10^8$ K s^{-1}) by an electric current pulse. All the properties of this carbide — specific heat, specific input energy, heat of melting — were obtained in the solid phase (from 2000 K and above); in the melting region ($T_m = 4300$ K); and in the liquid state (up to 5000 K). The temperature was measured from the radiation of the specimen surface by a high-speed pyrometer based on a high-speed photodetector PDA-10A (Thorlabs) calibrated using a temperature tungsten lamp.

The previously obtained experimental data on the maximum melting temperature of this compound (4300 K) relative to other refractory carbides (TaC and HfC) are confirmed. The specific heat of the carbide $Ta_{0.8}Hf_{0.2}C$ at high temperature begins to rise sharply for ≈ 400 K before precisely fixed melting starts. This confirms the assumption about the appearance of nonstationary Frenkel point defects in the lattice of a rapidly heated solid body in which the equilibrium concentration of vacancies does not have time to be established.

A target sintered by the SPS method was used to spray a carbide layer with a thickness of 1 μm on a K8 optical glass substrate with dimensions of $3.5 \times 8 \times 15$ mm. This layer adheres firmly to the surface of the substrate. K8 glass was chosen as a substrate due to the proximity of the coefficients of linear thermal expansion α: for K8 glass $\alpha = 7.1 \times 10^{-6}$ K^{-1}; for tantalum carbide $\alpha = (6.6-7.09) \times 10^{-6}$ K^{-1}; and for hafnium carbide $\alpha = 6.1 \times 10^{-6}$ K^{-1} (under normal conditions).

Formations with a diameter from 35 to 170 nm are visible on the mirror surface of the sprayed layer. They can be the

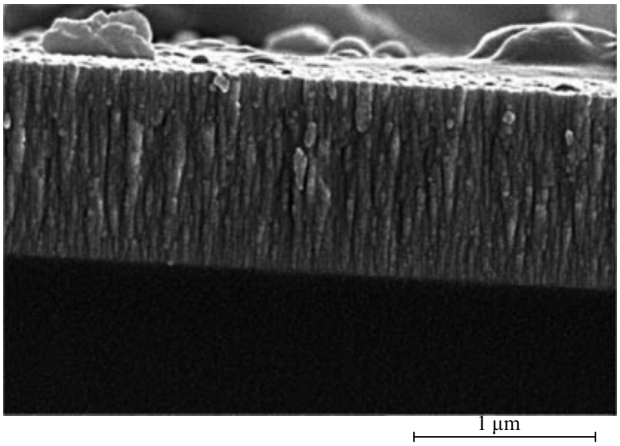

Figure 12. Columnar structure (in a fracture) of sprayed mixed TaC + HfC carbide, about 1 μm thick.

tops of a columnar structure (Fig. 12). The appearance of the assembled cell is shown in Fig. 13a. The side insulating plates are glued only for the initial retention of the cell. It should be noted that the value of the pulse pressure during the heating process depends on the material of the side plates and the quality of bonding. For example, if the side plates are made of glass, silica-glass, or sapphire, then their maximum impact strength increases by an order of magnitude (relative to stationary data). This makes it possible to study the thermophysical properties of conducting substances at high pressure [23]. That is why it is so important to show the cell design and its assembly in publications.

The result of an experiment with a sandwich-type specimen is shown in Fig. 13b. The decrease in radiation after the melting moment (arrow in Fig. 13b) is due to the fact that the molten surface of the carbide plate becomes more of a 'mirror' than it was before, the emissivity of the surface decreases, and then a melting plateau appears. The melting point (according to Fig. 13b) is ≈ 4300 K (that is, $T_{sol} \approx T_{liq}$).

Figure 14a shows the temperature dependence of the enthalpy $H(T)$ obtained by subtracting the energy losses spent on heating the substrate from the specific Joule heating energy E scattered in the specimen. We estimate this correction and heat losses in [24] for similar film specimens (composition ZrC + C) deposited on similar glass substrates (the specimen design was the same) for a temperature level of 3000 K and at the same heating time. Taking into account the similarity of the experimental conditions in [25] and in [24], we assume that the thermal losses for heating the substrate here are approximately the same as in [24], that is, 10% of the input energy. Taking into account this correction, the error of measuring input energy is $\approx 7\%$. Note that the input energy is actually the enthalpy H of the test specimen, since we may ignore a small increase in pressure when the specimen is heated and assume that heating occurs under quasi-isobaric conditions.

The error of measuring the heat of melting is 12%. The error of measuring the specific heat in this study is $\approx 15\%$ for the solid phase and $\approx 20\%$ for the liquid phase, except for the region of steep rise and fall of the specific heat before and after melting (Fig. 14b). The method of measuring the specific heat and the estimation of its error are described in detail in [28].

To calculate the true temperatures, we used the literature data on the normal spectral emissivity $\varepsilon_{n,\lambda}$ (the selection procedure is described in [29]). The temperature measurement error without taking into account the error $\varepsilon_{n,\lambda}$ was ± 50 K at a temperature of 3000 K and ± 80 K at 4700 K.

The temperature at the melting region (Fig. 14b) is close to 4300 K. The thermogram and temperature dependences of the properties differ from all the presented carbides — it can be recognized that the difference between T_{sol} and T_{liq} cannot be reliably measured for $Ta_{0.8}Hf_{0.2}C$ by the method under consideration.

A pseudobinar diagram of the TaC–HfC system, published by Gusev [92] in 1985, shows that, in the region of the maximum temperature of this compound (80 mol.% TaC + 20 mol.% HfC), the distance between the solidus and the liquidus of this compound is insignificant, which implies a small phase transition energy. Indeed, in our experiment, this energy is ≈ 0.54 kJ g^{-1}, which is close to the calculated value of the phase transition for TaC [65, 78].

The specific heat of solid carbide under pulsed heating in Fig. 14b is small (0.4 J g^{-1} K^{-1}) and coincides with previously

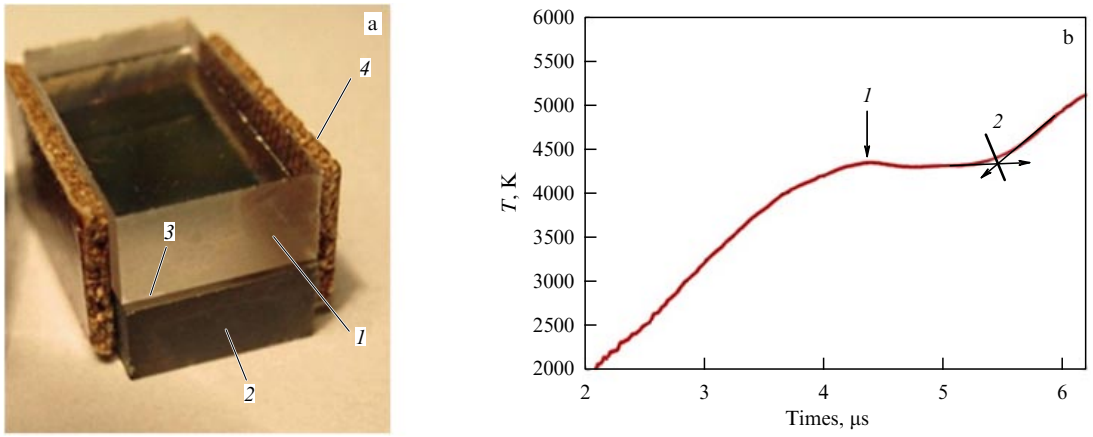

Figure 13. (a) Cell (sandwich type) to hold the carbide $Ta_{0.8}Hf_{0.2}C$ between plates (8 × 15 mm): *1* — top plate (silica-glass, 4 mm thick); *2* — bottom plate (K8 glass, 3.5 mm thick) with sprayed carbide; *3* — free belt for a contact of the specimen with electrode supply current (upper silica-glass is slightly shorter than the lower K8 plate); *4* — side plate (PCB) glued to initially hold the two glass plates. (b) Thermogram for one of the experiments. *1* — beginning of melting, solidus for carbide $Ta_{0.8}Hf_{0.2}C$ ($T_{sol} = 4300$ K); *2* — melting finish ($T_{liq} = 4300$ K). Decrease in temperature after the start of melting (arrow *1*) is due to the fact that the surface of the liquid phase of the specimen becomes perfectly smooth, which leads to a drop in its emissivity and radiation brightness.

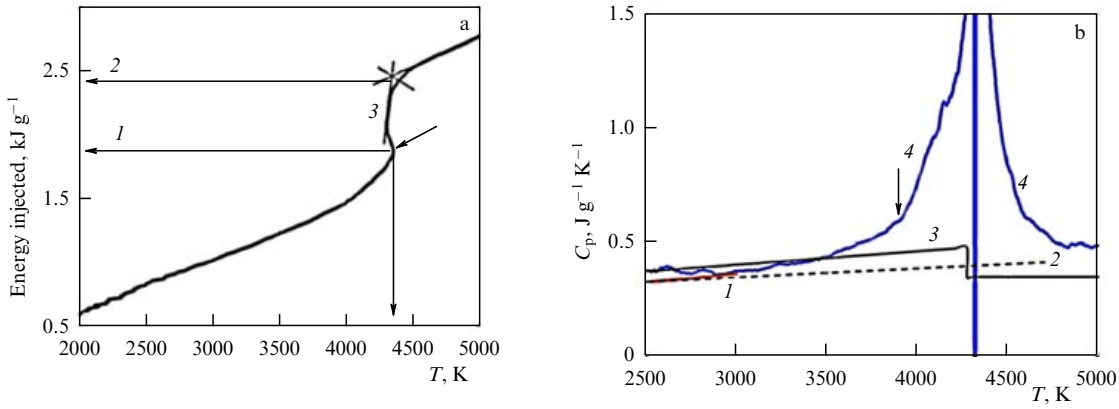

Figure 14. (a) Enthalpy of $Ta_{0.8}Hf_{0.2}C$ for one of the studied specimens is used to demonstrate a complex melting region. *1* — beginning of melting; *2* — end; *3* — melting area. Arrow shows the beginning of melting and a decrease in emissivity (the surface becomes more mirror-like), but this is not a drop in temperature. (b) Specific heat (close to C_p) depending on the temperature for $Ta_{0.8}Hf_{0.2}C$. Melting point is $\approx$ 4300 K (vertical line). Arrow indicates the temperature ($\approx$ 3900 K) at which the specific heat in the solid phase begins to increase sharply, and it takes place clearly long before melting. *1* — red line up to 3000 K — dependence of the specific heat of $Ta_{0.8}Hf_{0.2}C$ on temperature (calculation based on data on the specific heat of TaC and HfC [6]; *2* — data for TaC [78] (above 2843 K-extrapolation); *3* — data for TaC [65] (above 2761 K-extrapolation); *4* — data of our pulse experiment.

established data. It begins to increase long before melting (at a temperature of about 3500 K).

A faster increase in the specific heat is recorded at a temperature of 3900 K, that is, $\approx$ 300–400 K degrees before the melting begins (arrow in Fig. 14b). After melting, the specific heat of liquid carbide decreases faster than the previous growth in the solid phase and reaches close to the previous value at $\approx$ 300 K degrees after melting.

As a rule, the properties obtained by heating with a pulsed current are close to the equilibrium data. However, we observe a sharp increase in the specific heat in a narrow temperature range ($\approx$ 400 K before melting) for the $Ta_{0.8}Hf_{0.2}C$ carbide under study (Fig. 14b). As a hypothesis, it can be assumed that, with rapid heating, the formation of nonstationary defects occurs before melting. We assume that the reason for the observed increase in the specific heat before melting of rapidly heated substances is the occurrence of nonequilibrium defects in the lattice volume, leading to a loss of long-range order in the absence of a sufficient number of equilibrium vacancies. Saturation of the carbide with equilibrium vacancies along the diffusion path before melting is unlikely due to the slow steady state diffusion process. In the presence of Frenkel defects, the diffusion time may not be considered for the appearance of equilibrium vacancies, since, in the short time of the experiment, vacancies appear simultaneously with the appearance of interstitial atoms.

According to the experiment, relaxation of C_p in the liquid phase to its equilibrium values occurs within 1–2 μs. Thus, it can be concluded that the nonstationary defects under consideration are characterized by a 'lifetime' of about 1–2 μs.

We measured the melting point of this carbide and obtained 4300 ± 80 K, which, within the measurement error, coincides with the data for this composition obtained by the most reliable temperature measurement method based on the blackbody model [88]: $T_m = 4263$ K. It is impossible to agree with the remark made in [93] that these measurements may be erroneous due to the use of a correction during the transition from the observed temperature to the true one, since in [88] the true temperature was directly measured using the blackbody model. According to [88], the carbide $Ta_{0.8}Hf_{0.2}C$ has the highest melting point among (Ta, Hf)C carbides. Recognizing the reliability of the temperature measurements in [88], we confirm the result with our measurements (4300 K). At the same time, our measurements do not confirm the assumption in [88] that the highest melting point for $Ta_{0.8}Hf_{0.2}C$ is associated with the loss of carbon due to evaporation, since in our study evaporation was suppressed by the placement of mixed carbide between silica-glass plates and the short duration of the experiment. An indirect confirmation that this composition has the highest melting point is that, according to [94], it has the lowest evaporation rate at 2498–2998 K (it has the greatest stability) and, according to [91], the highest hardness among the carbides of the (Ta, Hf)C system (at 1873 K).

It should be noted that recently, in connection with the development of materials for extreme operating conditions, it has become of interest to search for substances with a maximum melting point. It is known in [20] that graphite is the most refractory substance ($T_m = 4900-5000$ K at not high pressures); however, graphite can be converted to the liquid phase only at a pressure above 120 bar [95]. In [96], based on the modeling of the properties of a substance by the method of molecular dynamics, a prediction was made that, among the known substances, hafnium carbonitride $Hf_{0.53}C_{0.27}N_{0.2}$ will have the highest melting point at atmospheric pressure. In [97], the first experiments were performed (without measuring the T_m itself), confirming an increase in the melting temperature for this composition compared to hafnium carbide.

A separate group of substances consists of so-called high-entropy carbides, which are mixed carbides based on several metals (usually more than 5) that are included in the alloy in approximately equal proportions by analogy with high-entropy alloys [98]. These carbides have a high melting point and unique new properties.

High-entropy carbides based on 5–7 metals of the IV–V groups of the periodic system of elements were produced in [98] by three different methods of SPS sintering at a temperature of 1900–2000 °C and a pressure of 60 MPa. The density of the resulting mixed carbides in some cases reached 100%. The resulting carbides had, in general, a single-phase cubic structure. The hardness measurements

showed that the composition including hafnium Hf (smaller grain size) has a higher hardness than the one including tungsten W. Apparently, the only method of studying their physical properties at high temperatures is pulsed current heating.

6. Electrical resistivity of carbides ZrC, ZrC + C, HfC, $Ta_{0.8}Hf_{0.2}C$ in solid and liquid states

It should be noted that, by resistivity, the authors understand the electrical resistance of a sample related to its initial dimensions (since the thermal expansion of carbides in this study was not measured). In the same experiment, both the thermophysical properties and the electrical resistance of the sample were measured. We applied the measurement technique described in [23]. The sample was heated to 5000 K for $\sim 5-10$ μs by passing a current pulse through it. The current $I(t)$, the voltage drop along the sample $U(t)$, and the signal from a high-speed pyrometer recording the radiance of the sample surface were measured using a Tektronix-3034 digital oscilloscope. The resistivity was calculated from the measured resistance of the sample $R = (U - L\,\mathrm{d}I/\mathrm{d}t)/I$ (L — inductance of the sample) and its initial geometric dimensions. Thermal losses of all types, chemical reactions with the environment, and changes in the composition of the sample can be disregarded due to the short time of the experiment. The temperature of a flat sample was measured by the radiation of its surface based on the literature data on the normal spectral emissivity of the material under study or by the radiation of a blackbody model made of this material [99]. In this study, all measurements were carried out using flat samples.

Two types of samples were studied (sintered, obtained by the SPS method, and one obtained by the magnetron sputtering method). The first method was used to obtain ZrC [25] and HfC samples; $Ta_{0.8}Hf_{0.2}C$ samples were obtained by the second method [29]. The electrical resistance of mixed carbide $Ta_{0.8}Hf_{0.2}C$ was studied in [100]. Methods for obtaining samples, as well as their characteristics, the cell designs, and the experimental conditions, are given in the previous sections of the review.

Table 2 shows the main characteristics of the carbides studied.

The dependence of the resistivity ρ for three carbides under study, including $Ta_{0.81}Hf_{0.19}C_{0.94}$ is shown in Fig. 15a. In contrast to HfC and ZrC (large crystallites), mixed carbide (small crystallites) demonstrates a positive increase in ρ to a clearly visible end of melting (Fig. 15a, horizontal arrow) [99].

The beginning of melting (T_{sol}) for ZrC was determined by the temperature dependence of the specific joule energy (enthalpy) and was 3440 K. The final melting point (T_{liq}) is 3850 K. The resistivity at these temperatures is $\rho = 290 \pm 20$ μΩ cm at the beginning of melting and 250 ± 20 μΩ cm at the end of melting. The resistivity of sintered ZrC at 3000 K is 320 μΩ cm (Fig. 15a), which is consistent with the data in [60] for sintered ZrC.

A comparison of the data in [24] for ZrC + C and in [25] for ZrC demonstrates the difference in the resistivity jump in the melting region of carbides: 700 and ≈ 900 μΩ cm for ZrC + C [24] and 290–250 μΩ cm for ZrC [25]. The higher resistivity in [24] can be explained by the presence of an excess of carbon in the ZrC + C samples (Table 1). Note that the resistivity of liquid carbon directly at the end of melting is ≈ 700 μΩ cm [20]. Recall that in all cases we are talking about the electrical resistivity related to the initial dimensions of the samples.

The electrical resistance of carbides with large crystallites (HfC and ZrC) under pulsed heating in the solid phase initially increases (up to $T \approx 0.80\ T_{\mathrm{sol}}$) and then decreases (Fig. 15a). It only grows in the liquid phase. The following Figure 15b shows the result of stationary heating of ZrC with large crystallites (heating and cooling). The dependence of electrical resistance versus temperature has the same form as with rapid heating. The reason in both cases (Fig. 15a and 15b) is the same — additional sintering during heating (improvement of the structure) due to incomplete initial sintering in the presence of large crystallites.

The temperature dependence of the resistivity in Fig. 15a and 15b can be explained by the fact that the sintering process of samples at 2100 K was not completed during their preparation and continued during the experiment at temperatures above 2100 K [101]. This results in a reduction in resistivity at higher temperatures.

An estimate of the time required for diffusion processes at grain boundaries gives $\tau \approx 10^{-5}-10^{-3}$ μs [99], i.e., at the heating durations under consideration (~ 5 μs, heating rate $\mathrm{d}T/\mathrm{d}t \sim 5 \times 10^8$ K s^{-1}), this time is sufficient for the diffusion rearrangement of grain boundaries.

The resistivity of the liquid phase of sintered carbides at the liquidus temperature is lower than or equal to that of the solid phase at the sintering temperature. Only for carbide obtained by magnetron sputtering does the dependence of $\rho(T)$ in the melting region change as it does for metals: it increases during melting compared to the solid-phase resistivity. Figure 16 shows the same electrical resistances, but depending on the specific input energy of joule heating E (in this case equal to enthalpy H).

Figure 16 even more definitely indicates the need to use samples of carbides with crystallites of a small initial size and more perfect structure, which show a continuous increase in electrical resistance over the entire heating range for both

Table 2. Initial characteristics of the investigated carbides.

Carbide	Initial density, g cm^{-3}	Porosity, %	Lattice parameter, nm	Grain size, μm	Manufacturing technology
ZrC + C [24]	~ 6.6	~ 1.5	0.4691	0.1	Magnetron sputtering
$ZrC_{0.95}$ [25]	6.57	~ 2.4	0.4694	2–15	SPS
$HfC_{0.85}$ [30]	12.45	~ 2.0	0.463451	15–20	SPS
$Ta_{0.81}\,Hf_{0.19}\,C_{0.94}$ [29, 100]	13.5	~ 4	0.450893	0.03–0.07	Magnetron sputtering

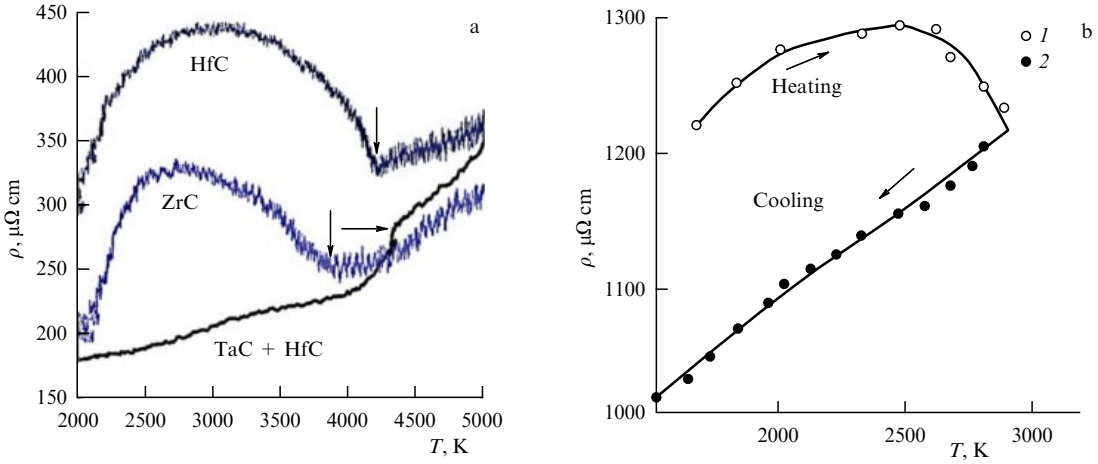

Figure 15. (a) Temperature dependences of resistivity for three carbides: HfC, ZrC, and TaC + HfC. Arrows indicate the end of melting (beginning of liquid state). In the liquid state, ρ for all carbides begins to increase linearly, like a metal-like substance [20]. (b) Change in resistivity for a $ZrC_{0.94}$ sample during a stationary experiment (porosity 42.5%, initial resistance 439 μΩ cm, lattice parameter 0.4691 nm): *1* — heating; *2* — cooling [101].

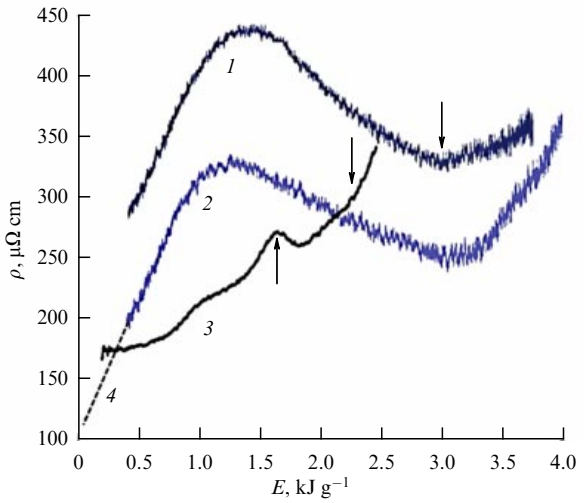

Figure 16. Dependence of electrical resistance on specific input energy E (enthalpy H) for three carbides: (*1*) HfC, (*2*) ZrC, and (*3*) TaC + HfC. Down arrows indicate the end of melting (beginning of liquid phase). Up arrow indicates the beginning of melting. (*4*) Linear extrapolation of the experimental values of electrical resistance to the initial conditions [99].

solid and liquid state of the carbide. Such resistance behavior ensures uniformity of energy input during pulse heating. Only for carbides with a small crystallite size (the curve for TaC + HfC carbide in Fig. 15a and curve *3* in Fig. 16) do the dependences of $\rho(T)$ and $\rho(E)$ in the melting region change as they do for metals: they increase during melting compared to the resistivity in the solid state.

A final conclusion may be as follows. In the pulsed heating process, it is desirable to use samples of carbides with a minimum size of the initial crystallites and with the most perfect structure. This will ensure uniform heating over a wide range of heating speeds (from tens of nanoseconds to hundreds of microseconds), while maintaining the metal-like solid and liquid phases. In connection with the above, we note that sol–gel synthesis when creating samples with a very small crystallite size [102] may be in demand for further experiments with pulsed heating. In the case of experiments with sintered samples of a large crystallite structure, it is desirable to sinter the samples at the highest possible temperature.

7. Properties of refractory carbides in the melting region

Comparative results for all carbides studied are shown in Table 3. The specific heat of C_p for the solid state is slightly higher than in stationary studies due to the presence of initial defects in the heated volume (samples were not annealed before the experiments).

We can draw the main conclusions from the consideration of the data in Table 3.

(1) The melting point of mixed carbide $Ta_{0.8}Hf_{0.2}C$ is slightly higher than for HfC (Table 3). However, the enthalpy of HfC carbide in the solid phase before melting and at the beginning of the liquid state is significantly higher than the enthalpy of mixed carbide in the same states, respectively: for HfC, 2.6 kJ g^{-1} and 3.4 kJ g^{-1}, and for $Ta_{0.8}Hf_{0.2}C$, 1.88 kJ g^{-1} and 2.42 kJ g^{-1}. This means that the HfC-based coating at close melting temperatures, all other things being equal, will begin to melt and break down at higher specific loads.

(2) Attention is drawn to the high enthalpy of the liquid phase of carbide (ZrC + C) 5.55 kJ g^{-1} and its high melting heat (3.2 kJ g^{-1}), which indicates the ability of such a coating to absorb significantly more energy during melting of equal mass than that of other carbides under consideration. This coating has additional advantages. First, the presence of an excess of carbon and its sublimation at relatively low pressures (of the order of atmospheric pressure) leads to the removal of part of the input energy and, accordingly, leads to cooling of the surface. At the moment, additional assessments are needed. Second, the relatively low density of the coating gives an advantage when using massive protective layers. In addition, as noted in [60], the presence of free carbon in the ZrC–C system improves the heat resistance and increases the erosion resistance of zirconium carbide when it is used in the nozzles of solid-fuel rockets.

(3) According to Table 3, mixed carbide $Ta_{0.8}Hf_{0.2}C$ has the highest molar enthalpy for solid and liquid states (as well as the highest melting point, 4300 K).

8. Conclusion

In addition to the advantages of the method of rapid electric heating, noted at the beginning of the review, we will point out

Table 3. Comparative experimental results for all carbides investigated.

Carbide, manufacturing, content, at.%	Density, g cm^{-3}/mol (g)	Enthalpy H_{sol}, kJ g^{-1}/kJ mol^{-1}	Enthalpy H_{liq}, kJ g^{-1}/kJ mol^{-1}	$\Delta H = H_{liq} - H_{sol}$, kJ g^{-1}/kJ mol^{-1}	T_{sol}/T_{liq}, K	C_p, (solid.), J g^{-1} K^{-1}/ J mol^{-1} K^{-1}	C_p (liq.), J g^{-1} K^{-1}/ J mol^{-1} K^{-1}
ZrC + C sputtering Zr — 17.88; C — 67.69; N — 8.13; O — 6.0	4.3/103	2.35/242 at 3150 K	5.55/572 at 3640 K	3.2/330	3150/3640	$\sim 0.85/\sim 88$ at 2700 K	$\sim 0.6/\sim 62$ at 5000 K
ZrC sintered Zr — 47.4; C — 45.0; Hf — 0.4; N — 3.4; O — 3	6.57/103	2.2/227 at 3450 K	3.3/340 at 3850 K	1.1/113	3440/3850	$\sim 1.0/\sim 103$ at 3000 K	$\sim 0.7/\sim 72$ at 4500–5000 K
$Ta_{0.8}Hf_{0.2}C$ sputtering Ta — 41.23; Hf — 9.42; C — 48.83	13.5/360	1.88/677 at 4300 K	2.42/871 at $\sim$ 4400 K	0.54/194	$\sim$ 4300/4300	$\sim 0.4/\sim 144$ at 3000 K	$\sim 0.5/\sim 180$ at 5000 K
HfC sintered Hf — 49; C — 42; O — 7	12.45/191	2.6/497 at 4000 K	3.4/649 at 4200 K	0.8/152	4100/4200	$\sim 0.7/\sim 134$ at 3000 K	$\leqslant 0.5/\leqslant 96$ at 5000 K

the features of this method (which became clear only after practical experience of its application).

1. It is established that the specific heat of carbides in the solid state (in a wide temperature range) may be slightly higher than the data obtained in stationary experiments. With rapid heating, the initial lattice defects and impurities remain in the unburned sample until the liquid state is reached. This leads to a slightly higher specific heat of the solid sample. (Sometimes, the additional energy associated with an increase in the specific heat is within the uncertainty of the enthalpy measurements: from 5 to 7%).

The validity of this statement is supported by the fact that rapid current heating of quasi-crystalline anisotropic graphite with a purity of 99.99% (i.e, with a small number of impurities and defects) gives the specific heat of the solid phase, which coincides with the specific heat during stationary heating [20]. It can be expected that preliminary annealing of carbide samples before experiments with rapid heating will lead to a decrease in the difference in the values of the specific heat of the solid phase obtained by the methods of rapid and stationary heating.

2. A sharp increase in the specific heat is observed with rapid heating of all the substances under study — metals, alloys, graphite, and carbides — immediately before melting. This steep increase in the specific heat, according to our assumption, is caused by the appearance of point defects (for example, paired Frenkel defects). With rapid heating, it is impossible to saturate the lattice with equilibrium vacancies in order to ensure the loss of long-range order during melting. Our approach to understanding the physics of the solid and liquid state of matter is based on the work of J I Frenkel [66].

Despite the fact that we have been talking about this physical effect for 30 years, we have not seen contemporary studies by theorists who pay attention to it. Recently, similar papers have begun to appear. Note the computational work [21], in which molecular dynamic modeling of ZrC was carried out using the density functional theory, which showed the spontaneous formation of Frenkel pair defects at a temperature of 3200 K, about 500 K below the melting point of ZrC. The conclusions of [21] indicate that a high concentration of Frenkel defects changes the properties of ZrC in several important ways. According to [21], the formation of one defect for every 64 atoms of a ZrC cell approximately doubles the electron density of states at the Fermi level, reduces the bulk modulus of elasticity by 8–18 GPa, and expands the lattice by 0.1–0.15%. The contribution of Frenkel defects to the specific heat is relatively small for moderate temperatures $T < 2000$ K, but it is assumed that it will be much larger near the melting point [21].

3. In this regard, it is also necessary to point out another effect observed with rapid heating of a conductor (in particular, metal). Simultaneously with an increase in the specific heat, abnormally large electron emission occurs before melting [19, 103]. First, it should be noted that the melting point of the substance does not depend on the high heating rate. With rapid heating, an excessive increase in the input energy of joule heating before melting is recorded. However, the excess of the input energy by the beginning of melting does not go to increase the temperature, but is absorbed by the lattice, changing its properties [30]. Second, an increase in the specific heat before melting of the metal occurs simultaneously with the appearance of abnormally large electron emission from a solid metal [19, 103]. It can be assumed that the same effect of anomalous electron emission occurs during rapid heating of carbides with metallic conductivity. The appearance of these two physical effects (abnormally high specific heat and increased electron emission) occurring before the melting of a rapidly heated substance should attract the attention of both experimenters and theorists.

4. In recent years, there have been studied on the properties of refractory systems using joint computational and experimental techniques. In review [104], phase equilibria of complex Hf–Zr–C–N–O systems are considered, with an emphasis on carbides and carbonitrides of Zr and Hf, in order to predict the most refractory compounds.

In [97], it was possible in a stationary experiment to obtain a comparative estimate of the melting temperature of the created carbonitride ceramics HfCN and the melting temperature of carbide HfC. With simultaneous (quasi-stationary) heating of two compounds, it was noticed that HfC began to melt earlier than the synthesized carbonitride

$HfC_{0.5}N_{0.35}$. This allowed the authors of [97] to conclude that the carbonitride they created had a higher melting point than HfC.

Note that the computational approaches still do not allow us to obtain the thermophysical properties of these compounds in the liquid state, especially their dependence on temperature. In experiments with stationary heating, the measurement of such properties is very difficult or impossible. Only pulsed current heating can be used here. It should be noted that the use of laser pulse heating is successfully used to study the temperature parameters of phase diagrams of carbides in their melting region [87].

It is obvious that further experiments involving heating by a current pulse with temperature measurements (up to 6000 K) can be planned with the composition of the samples recommended in [104, 97]. At the same time, the main problem is to create targets and further magnetron sputtering of thin coatings (about 5–15 μm) for their use in creating samples in the form of a blackbody model. This is due to the fact that, for all new compounds, the emissivity values are not available in the literature, and pulsed heating of samples in the form of a blackbody model makes it possible to measure their true temperature using an estimation of this value [33].

Not so long ago, research was started on a new class of alloys called high-entropy alloys [98, 105, 106]. Unlike classical alloys having a base element and alloying elements, high-entropy alloys contain a significant number of elements (from 5 to 12–15) introduced in equal or close to equal proportions. In these alloys, due to a large degree of disorder and a large amount of configuration entropy, there is a predominant formation of a solid solution based on crystal lattices of bcc or hcc. It is the entropy contribution that determines the properties of these alloys. We expect that pulsed current heating can provide new knowledge in the study of highly entropic substances based on mixed compounds of several metals, including several carbides [107–109].

This article was prepared in 2021 with the financial support of the Russian Foundation for Basic Research (RFBR), grant no. 19-08-00093.

Acknowledgments. The authors are grateful to T I Borodina, G E Valiano, S A Evdokimov, and P N Medvedev for the production and microstructural, elemental, and X-ray diffraction analyses of samples.

References

1. Wuchina E et al. *Electrochem. Soc. Interface* **16** 30 (2007)
2. Mungiguerra S et al., in *2018 Intern. Energy Conversion Engineering Conf., July 2018* (Session: Thermal System Applications and Unique Environment III) (Reston, VA: American Institute of Aeronautics and Astronautics, 2018) AIAA 2018-4694, https://doi.org/10.2514/6.2018-4694
3. Zeng Y et al. *Nat. Commun.* **8** 15836 (2017)
4. Andrievski R A *Phys. Usp.* **60** 276 (2017); *Usp. Fiz. Nauk* **187** 296 (2017)
5. Andrievski R A *Phys. Usp.* **57** 945 (2014); *Usp. Fiz. Nauk* **184** 1017 (2014)
6. Storms E K *The Refractory Carbides* (New York: Academic Press, 1967)
7. Kosolapova T Ya *Carbides*; *Properties, Production, and Applications* (New York: Plenum Press, 1971); Translated from Russian: *Karbidy* (Moscow: Metallurgiya, 1968)
8. Toth L E *Transition Metal Carbides and Nitrides* (New York: Academic Press, 1971)
9. Samsonov G V, Upadkhaya G Sh, Neshpor V S *Fizicheskoe Materialovedenie Karbidov* (Physical Materials Science of Carbides) (Kiev: Naukova Dumka, 1974)
10. Pierson H O *Handbook of Refractory Carbides and Nitrides*: *Properties*, *Characteristics*, *Processing*, *and Applications* (Park Ridge, NJ: Noyes Publ., 1996)
11. Krzhizhanovskii R E, Shtern Z Yu *Teplofizicheskie Svoistva Nemetallicheskikh Materialov. Karbidy*. Spravochnaya Kniga (ThermoPhysical Properties of Non-Metallic Materials. Carbides. Reference Book) (Leningrad: Energiya, 1977)
12. Kotel'nikov R B et al. *Osobo Tugoplavkie Elementy i Soedineniya*. Spravochnik (Particularly Refractory Elements and Compounds. Handbook) (Moscow: Metallurgiya, 1969)
13. Shabalin I L *Ultra-High Temperature Materials II. Refractory Carbides I* (Ta, Hf, Nb *and* Zr *Carbides*) (Dordrecht: Springer, 2019) https://doi.org/10.1007/978-94-024-1302-1
14. Touloukian Y S (Series Ed.) *Thermophysical Properties of Matter* (New York: IFI/Plenum, 1970 – 1979)
15. Allen P B *Phys. Rev. Lett.* **59** 1460 (1987)
16. Brorson S D et al. *Phys. Rev. Lett.* **64** 2172 (1990)
17. Onufriev S V, Savvatimskiy A I, Kondratyev A M *High Temp. High Press.* **43** 217 (2014)
18. Eggert J H et al. *Nat. Phys.* **6** 40 (2010)
19. Lebedev S V, Savvatimskii A I *Sov. Phys. Usp.* **27** 749 (1984); *Usp. Fiz. Nauk* **144** 215 (1984)
20. Savvatimskii A I, Onufriev S V *Phys. Usp.* **63** 1015 (2020); *Usp. Fiz. Nauk* **190** 1085 (2020)
21. Mellan T A, Duff A I, Finnis M W *Phys. Rev. B* **98** 174116 (2018)
22. Savvatimskiy A I, Korobenko V N *Vysokotemperaturnye Svoistva Metallov Atomnoi Energetiki*: *Tsirkonii, Gafnii i Zhelezo pri Plavlenii i v Zhidkom Sostoyanii* (High-Temperature Properties of Nuclear Energy Metals: Zirconium, Hafnium and Iron during Melting and in the Liquid State) (Moscow: Izd. Dom MEI, 2012)
23. Savvatimskiy A I, Onufriev S V *Phys. Atom. Nucl.* **79** 1637 (2016); *Yad. Fiz. Inzhiniring* **6** 622 (2015)
24. Kondratyev A et al. *J. Alloys Compd.* **631** 52 (2015)
25. Savvatimskiy A I, Onufriev S V, Muboyadzhyan S A *J. Mater. Res.* **32** 1287 (2017)
26. Savvatimskiy A I et al. *J. Phys. Conf. Ser.* **891** 012318 (2017)
27. Savvatimskiy A I et al. *Bull. Russ. Acad. Sci. Phys.* **82** 363 (2018); *Izv. Ross. Akad. Nauk Fiz.* **82** 419 (2018)
28. Savvatimskiy A I *High Temp.* **56** 678 (2018); *Teplofiz. Vys. Temp.* **56** 704 (2018)
29. Savvatimskiy A I, Onufriev S V, Muboyadzhyan S A *J. Europ. Ceram. Soc.* **39** 907 (2019)
30. Savvatimskiy A I et al. *J. Mater. Sci.* **55** 13559 (2020)
31. Aristova N M, Onufriev S V, Savvatimskiy A I *High Temp.* **58** 681 (2020); *Teplofiz. Vys. Temp.* **58** 749 (2020)
32. Buchnev L M et al. *Sov. Phys. Dokl.* **29** 837 (1984); *Dokl. Akad. Nauk SSSR* **278** 1109 (1984)
33. Onufriev S V *Bull. Russ. Acad. Sci. Phys.* **82** 372 (2018); *Izv. Ross. Akad. Nauk Fiz.* **82** 430 (2018)
34. Korobenko V N, Rakhel A D *Int. J. Thermophys.* **20** 1257 (1999)
35. Grigoriev I S, Meilikhov E Z (Eds) *Handbook of Physical Quantities* (Boca Raton, FL: CRC Press, 1997); Translated from Russian: *Fizicheskie Velichiny*. Spravochnik (Moscow: Energoatomizdat, 1991)
36. Varshney D, Shriya S *Int. J. Refract. Met. Hard Mater.* **41** 375 (2013)
37. Onufriev S V, Savvatimskiy A I, Muboyadzhyan S A *Mater. Res. Express* **6** 125554 (2019)
38. Polezhaev Yu V, Yurevich F B *Teplovaya Zashchita* (Thermal Protection) (Ed. A V Lykov) (Moscow: Energiya, 1976)
39. Aristova N M, Belov G V *High Temp.* **60** (1) (2022); *Teplofiz. Vys. Temp.* **60** 23 (2022)
40. Neel D S, Pears C D, Oglesby S (Jr.) "The thermal properties of thirteen solid materials to 5000F for their destruction temperatures", Technical Report WADD-TR-60-924 (Birmingham, AL: Southern Research Institute, 1962); http://contrails.iit.edu/reports/AD0275536
41. Westrum E F (Jr.), Feick G *J. Chem. Eng. Data* **8** 176 (1963)
42. McClaine L A (Ed.) "Thermodynamic and kinetic studies for a refractory materials program", Technical Report No. ASD-TDR-

62-204, Pt. 2 (Cambridge, MA: Arthur D. Little, Inc, 1962); http://contrails.iit.edu/reports/7395
43. Levinson L S *J. Chem. Phys.* **42** 2891 (1965)
44. Kantor P B, Fomichev E N *High Temp.* **5** 41 (1967); *Teplofiz. Vys. Temp.* **5** 48 (1967)
45. Bolgar A S, Guseva E A, Fesenko V V *Poroshk. Metallurg.* (1) 40 (1967)
46. Turchanin A G, Fesenko V V *Poroshk. Metallurg.* (1) 88 (1968)
47. Sheindlin A E, Belevich I S, Kozhevnikov I G *High Temp.* **11** 599 (1973); *Teplofiz. Vys. Temp.* **11** 666 (1973)
48. Mebed M M, Yurchak R P, Korolev L A *High Temp.* **11** 380 (1973); *Teplofiz. Vys. Temp.* **11** 427 (1973)
49. Korshunov I G et al. *High Temp.* **15** 439 (1977); *Teplofiz. Vys. Temp.* **15** 521 (1977)
50. Petrova I I, Chekhovskoi N Y *High Temp.* **16** 1045 (1978); *Teplofiz. Vys. Temp.* **16** 1226 (1978)
51. Bolgar A S et al. "Termodinamicheskie svoistva karbida tsirkoniya v oblasti gomogennosti" ("Thermodynamic properties of zirconium carbide in the region of homogeneity") (Kiev, 1989), All-Russian Institute for Scientific and Technical Information, Deposit No. 1162-V89
52. Aristova N M *Russ. J. Phys. Chem. A* **94** 2685 (2020)
53. Turchanin A G, Fesenko V V *Poroshk. Metallurg.* (6) 48 (1969)
54. Storms E K, Wagner P *High Temp. Sci.* **5** 454 (1973)
55. Storms E K, Griffin J *High Temp. Sci.* **5** 291 (1973)
56. Tshai V A *Zh. Fiz. Khim.* **64** 689 (1990)
57. Tshai V A *Zh. Fiz. Khim.* **64** 2354 (1990)
58. Fernández Guillermet A *J. Alloys Compd.* **217** 69 (1995)
59. Hugosson H W et al. *Chem. Phys. Lett.* **333** 444 (2001)
60. Jackson H F, Lee W E, in *Comprehensive Nuclear Materials* (Ed.-in-Chief R J M Konings) (Amsterdam: Elsevier, 2012) p. 339
61. Katoh Y et al. *J. Nucl. Mater.* **441** 718 (2013)
62. Xie C et al. *Phys. Chem. Chem. Phys.* **18** 12299 (2016)
63. Jiang M et al. *Sci. Rep.* **7** 9344 (2017)
64. Gasparrini C et al. *Sci. Rep.* **10** 6347 (2020)
65. Schick H L (Ed.) *Thermodynamics of Certain Refractory Compounds* Vol. 1, 2 (New York: Academic Press, 1966)
66. Frenkel J *Kinetic Theory of Liquids* (Oxford: The Clarendon Press, 1946); Translated from Russian: *Kineticheskaya Teoriya Zhidkostei* (Leningrad: Nauka, 1975)
67. Zapadaeva T E, Petrov V A, Sokolov V V *High Temp.* **19** 228 (1981); *Teplofiz. Vys. Temp.* **19** 313 (1981)
68. Korobenko V N, Savvatimskiy A I *Russ. J. Phys. Chem.* **77** 1564 (2003)
69. Korobenko V N, Savvatimskiy A I *High Temp.* **45** 159 (2007); *Teplofiz. Vys. Temp.* **45** 187 (2007)
70. Korobenko V N, Savvatimskiy A I *AIP Conf. Proc.* **684** 783 (2003)
71. Savvatimskiy A I *Carbon* **43** 1115 (2005)
72. Savvatimskiy A I *J. Phys. Condens. Matter* **20** 114112 (2008)
73. Savvatimskiy A *Carbon at High Temperatures* (Springer Ser. in Materials Science, Vol. 134) (Cham: Springer, 2015) https://doi.org/10.1007/978-3-319-21350-7
74. Manara D et al. *J. Eur. Ceramic Soc.* **33** 1349 (2013)
75. Onufriev S V, Savvatimskii A I, Yanchuk V I *Izmerit. Tekh.* (8) 49 (2011)
76. Korobenko V N "Eksperimental'noe issledovanie svoistv zhidkikh metallov i ugleroda pri vysokikh temperaturakh" ("Experimental investigation of the properties of liquid metals and carbon at high temperatures"), Ph.D. Thesis (Phys.-Math. Sci.) (Moscow: Joint Institute for High Temperatures of the Russian Academy of Sciences, 2001)
77. Reithof T, Acchione B D, Branyan E R, in *Temperature, Its Measurement and Control in Science and Industry* Vol. 3 (Ed. C M Herzfeld) Pt. 2 *Applied Methods and Instruments* (Ed. A I Dahl) (New York: Reinhold, 1967) p. 515
78. Chase M W (Ed.) *NIST-JANAF Themochemical Tables* (J. Phys. Chem. Ref. Data, Monograph, No. 9) 4th ed. (Woodbury, NY: American Institute of Physics for the National Institute of Standards and Technology, 1998) p. 652
79. Bolgar A S, Turchanin A G, Fesenko V V *Termodinamicheskie Svoistva Karbidov* (Thermodynamic Properties of Carbides) (Kiev: Naukova Dumka, 1973)
80. Turchanin A G *Russ. J. Phys. Chem. A* **54** 2962 (1980)
81. Barin I *Thermochemical Data of Pure Substances* Vol. 1, 2, 3rd ed. (Weinheim: VCH, 1995)
82. Bgasheva T et al., in *CALPHAD XLIV Intern. Conf. Computer Coupling of Phase Diagrams and Thermochemistry Calphad XLIV, May 31 – June 5, 2015 Loano, Italy*
83. Levinson L S *J. Chem. Phys.* **40** 1437 (1964)
84. Guseva E A *Russ. J. Phys. Chem. A* **45** 2948 (1971)
85. Knyazkov A M et al. *High Temp. High Press.* **40** (3 – 4) 349 (2011)
86. Zapadaeva T E, Petrov V A, Sokolov V V *High Temp.* **18** 68 (1980); *Teplofiz. Vys. Temp.* **18** 76 (1980)
87. Sheindlin M et al. *Adv. Appl. Ceram.* **117** (S1) s48 (2018)
88. Andrievskii R A et al. *Sov. Powder Metallurg. Metal Ceram.* **6** (1) 65 (1967); *Poroshk. Metallurg.* (1) 85 (1967)
89. Cedillos-Barraza O et al. *Sci. Rep.* **6** 37962 (2016)
90. Klimov D A et al. *Tr. Mosk. Aviats. Inst.* (46) ID 6 (2011); https://trudymai.ru/published.php?ID = 26114
91. Osama Gaballa Gaballa Processing Development of 4TaC-HfC and Related Carbides and Borides for Extreme Environments, Graduate Theses and Dissertations, Iowa State University (2012)
92. Gusev A I *Russ. J. Phys. Chem.* **59** 336 (1985); *Zh. Fiz. Khim.* **59** 579 (1985)
93. Arblaster J *Anal. Bioanal. Chem.* **407** 6589 (2015)
94. Deadmore D L *J. Am. Cer. Soc.* **48** 357 (1965)
95. Gokcen N A et al. *High Temp. Sci.* **8** 81 (1976)
96. Hong Q-J, van de Walle A *Phys. Rev. B* **92** 020104 (2015)
97. Buinevich V S et al. *Ceramics Int.* **46** (10) 16068 (2020)
98. Potschke J et al. *J. Mater. Sci.* **56** 11237 (2021)
99. Savvatimskii A I, Onufriev S V *High Temp.* **58** 778 (2020); *Teplofiz. Vys. Temp.* **58** 865 (2020)
100. Savvatimskii A I, Onufriev S V *High Temp.* **57** 140 (2019)
101. Vishnevetskaya I A et al. *High Temp.* **18** 414 (1980); *Teplofiz. Vys. Temp.* **18** 523 (1980)
102. Simonenko E P "Novye podkhody k sintezu tugoplavkikh nanokristallicheskikh karbidov i oksidov i polucheniyu ul'travysokotemperaturnykh keramicheskikh materialov na osnove diborida gafniya" ("New approaches to the synthesis of refractory nanocrystalline carbides and oxides and the production of ultrahigh-temperature ceramic materials based on hafnium diboride"), Abstract of Doctoral Thesis (Chem. Sci.) (Moscow: Kurnakov Inst. of General and Inorganic Chemistry of the RAS, 2016)
103. Lebedev S V, Khaikin S E *Zh. Eksp. Teor. Fiz.* **26** 723 (1954)
104. Ushakov S V et al. *Materials* **12** 2728 (2019)
105. Wissner-Gross A D, Freer C E *Phys. Rev. Lett.* **110** 168702 (2013)
106. Yeh J-W et al. *Adv. Eng. Mater.* **6** 299 (2004)
107. Savchenko A "Entropiinye effekty v real'nykh sistemakh" ("Entropy effects in real systems") *Atomnaya Strategiya* **110** 14 (2015); http://www.proatom.ru/modules.php?name = News&file = print&sid = 6440
108. Savchenko A *Energy Nature of Configurational Entropy. Generation of Entropy and Anti-entropy Flows* (Saarbrucken: LAMBERT, 2015)
109. Fernandes C M, Senos A M R *Int. J. Refract. Met. Hard Mater.* **29** 405 (2011)